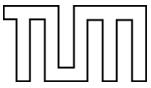

Technische Universität München

Department of Mathematics

Master's Thesis

Mathematical Modeling of the Cooperation Dynamics of *Pseudomonas Aeruginosa* Populations

Michael Blasi

Supervisor: Prof. Dr. C. Kuttler

Advisor: Dr. J. Pérez-Velázquez

Submission Date: 15 June 2015

I assure the single handed composition of this master's thesis is only supported by declared resources.

Garching,

Zusammenfassung

In der beiligenden Arbeit wird das Gram-negative Bakterium *Pseudomonas aeruginosa* vorgestellt, welches schwere Infektionen im Menschen auslösen kann. Diese Bakterienart verwendet eine Strategie, die Quorum sensing bezeichnet wird. Bakterien die diese Strategie nutzen senden Signalmoleküle, die Autoinducer genannt werden, in ihre Umgebung aus, was bei einer großen Autoinducerkonzentration zu einer gezielten Genexpression führen kann. Die Bakterien agieren hierbei ähnlich einem mehrzelligen Organismus und produzieren Produkte, die von anderen Zellen mitgenutzt werden. Dieses kooperative Verhalten wird durch sogenannte Cheaterzellen ausgenutzt, indem diese von den Produkten profitieren, ohne eigene Produkte für die Gemeinschaft herzustellen. Auf die Frage, warum sich Quorum sensing als Strategie halten konnte, wird in der Arbeit noch näher eingegangen. Weiterhin werden mathematische Modelle vorgestellt, die die Dynamik von Cheater- und Wildtypzellen beschreiben, welche zusammen unter verschiedenen Startverhältnissen wachsen, um zu untersuchen wie diese miteinander interagieren. Daraufhin führen wir eine Modellselektion durch, die auf den zu verfügbaren Daten beruht. Weiterhin können wir einige Parameter von biologischer Signifikanz bestimmen, wie etwa Wachstumsraten.

Abstract

In the following work, mathematical models for the cooperative dynamics of the Gram-negative bacterium *Pseudomonas aeruginosa* will be presented, which is a pathogen that can cause severe infections. This bacterium uses a strategy called quorum sensing. Bacteria using this strategy emit signal molecules, called autoinducers, to their environment, which lead to the expression of specific genes at high autoinducer density. Bacteria, in this way, act similar to a multicellular organism and produce products, which other cells can use. This cooperative behavior can be exploited by so called cheater cells, which profit from those products without producing own products for the community. The question arises, why quorum sensing exists as a strategy, which will be discussed in the work later. Furthermore we present mathematical models of the dynamics of cheater and wildtype cells, growing together under diverse initial proportions, to explore how they interact. We then perform a model selection based on the experimental data available. We are further able to estimate some parameters of biological significance such as growth rates.

Contents

1. Introduction

Bacteria that develop resistance to antibiotics have been a big risk for humanity since years. Britain's chief medical officer Sally Davies for example stated that this problem should be added to the list of national emergencies and mentioned: "there are few public health issues of potentially greater importance for society than antibiotic resistance" [25]. Margaret Chan, the director-general of the WHO, stated: "In terms of new replacement antibiotics, the pipeline is virtually dry, especially for Gram-negative bacteria". [13]. She also noted that we are fast approaching a post-antibiotic era and "an end to modern medicine, when things as common as a strep throat or a child's scratched knee could once again kill". It is, therefore, of great importance to develop alternative methods to inhibit bacterial virulence. The development of drugs interfering with quorum sensing, a process that bacteria use to communicate, is a promising new research area. This could be of considerable medical value given the continuing increase in resistance to antibiotics exhibited by many pathogenic species, including *Pseudomonas aeruginosa* [11].
Quorum sensing can be exploited by mutated cells benefiting from products segregated by the cooperating cells without producing so called "public goods" on their own, and thus exploiting this cooperative behavior [21]. In the following we focus on this exploitative behavior in the *Pseudomonas aeruginosa* bacteria, which is one of the top three causes of infections in which bacteria take advantage of their host having a weakened immune system [5]. We focus on the dynamics of the PA14 wildtype cells and mutated cells that exploit the cooperative behavior of the wildtype cells. We develop models to explore the dynamics of both populations, i. e. wildtype (PA14) and cheater cells based on standard models of interacting populations and fit data to several models to find an appropriate description of this interaction. In the biological background part (see chapter 2) we introduce the process of quorum sensing, and in particular quorum sensing in *Pseudomonas aeruginosa*. We also explain the exploitation of quorum sensing by cells, such as the mutated cells mentioned above. In chapter 3, we introduce some well-known mathematical models. Moreover we introduce some mathematical basics that we need for the fitting procedure of the models and for the analysis. In chapter 4, we formulate models that we base on theory and existing models and that are analyzed in chapter 5. In chapter 6 some future work is mentioned that can be done on this topic.

2. Biological Background

In the following we introduce the process of quorum sensing and in particular describe the underlying quorum sensing systems in *Pseudomonas aeruginosa*. We describe the exploitative behavior of cells that benefit from the public goods produced by cells participating in quorum sensing. Afterwards, we introduce some mathematical models and mathematical techniques that we use for the analysis.

2.1. Quorum Sensing in Pseudomonas Aeruginosa

Quorum sensing is a communication process between bacterial cells that includes the production, detection and response to extracellular signaling molecules called autoinducers [29]. The autoinducer concentration increases in the environment of bacteria with an increasing number of bacterial cells, which produce them and send them out in the environment [24]. Surrounding cells can monitor the concentration of autoinducers and when a specific threshold of autoinducer concentration is reached, the bacterial cells express specific genes, which lead to the formation of biofilms and virulence factor emission [19]. All known bacterial cells using quorum sensing follow three basic behaviors: First, the cells participating in quorum sensing produce autoinducers. When the cell density in the environment is low, the autoinducers are present at concentrations that the bacterial cells cannot detect [2]. At high cell density, the bacterial cells can identify the autoinducers. Secondly, the autoinducers can be detected by receptors that are present in the cytoplasm or in the cell membrane. Thirdly, the detection of autoinducers results in the activation of autoinducer production, leading to a feed-forward loop [29].
In this work we study the Gram-negative bacterium *Pseudomonas aeruginosa*. *Pseudomonas aeruginosa* can cause acute and chronic infections in humans [16]. Typically, infections with *Pseudomonas aeruginosa* depend on the host having a compromised immune system. The bacterium is responsible for a considerable amount of urinary tract infections, and also one of the most common lethal pathogens in intubated patients [10]. Up to 10% of the genome is controlled by quorum sensing [17]. There are three known quorum sensing systems that appear in the Gram-negative bacterium *Pseudomonas aeruginosa*, two quorum sensing circuits that control the expression of virulence factors as well

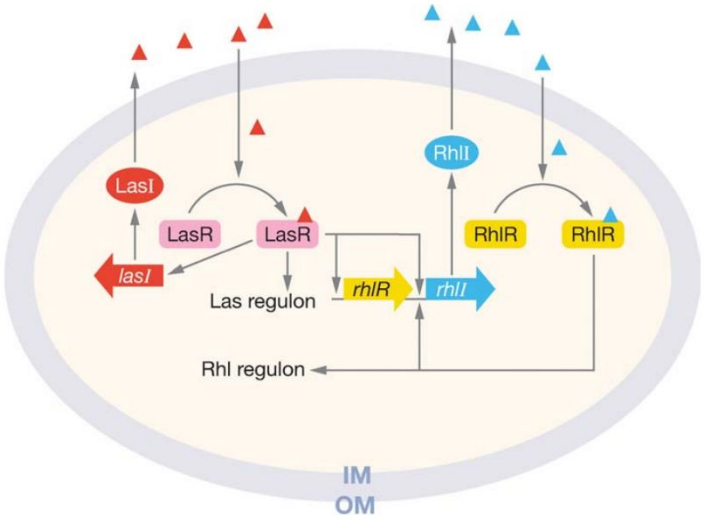

Figure 2.1.: The synthase LasI synthesizes the autoinducer 3-oxo-C12-homoserine lactone, represented by the small red triangles. Those autoinducers form a complex with LasR. Since lasI is also a target, this leads to an autoinducing feed-forward loop. The rhlI region is also a target, leading to a feed-forward loop in the second quorum sensing circuit. The blue triangles represent butanoyl homoserine lactone. The picture is adopted from Waters and Bassler [6].

as a third system called the Pseudomonas quinolone signal system [29]. In the first one, the autoinducer synthase LasI synthesizes 3-oxo-C12-homoserine lactone [31]. When the concentration of cells reaches a specific threshold, this autoinducer forms a complex with a protein called LasR [18]. This complex leads to a transcription of specific genes that encode virulence factors [28]. One of the LasR-3-oxo-C12-homoserine lactone targets is lasI, resulting in an autoinducing feed-forward loop [20]. Another target of the lasR-3-oxo-C12-homoserine lactone complex is called rhlI, and the according autoinducer synthase RhlI synthesizes the autoinducer called butanoyl homoserine lactone [4]. Since rhlI is a target of this complex as well, the result is again an autoinduction [22]. In figure 2.1, the mechanism we described is depicted. We do not explain the Pseudomonas quinolone signal system in detail, however, further information can be found in Rutherford and Bassler [29].

2.2. Exploitation of Quorum Sensing by Social Cheater Cells

The cooperative behavior of bacteria participating in quorum sensing is susceptible to exploitation by social cheaters. Those cheaters benefit from the products secreted by the cooperators without producing the same amount of "public goods" for the community [21]. In the tragedy of the commons, something similar happens. When an area gets used by a group of herdsmen, the best strategy for an individual herdsmen is to hold as many animals as possible, even if this leads to a destructed ground. The dilemma is, that the prize for renewing the ground is shared among all of the herdsmen. Thus, the individual herdsman has an advantage, but the disadvantage is shared among all of them. Therefore, although cooperation would be advantageous for the whole group, the outcome is a breakdown of the cooperation [30]. The interesting fact about the strategy of quorum sensing is that those social cheaters arise, which exploit this cooperative behavior, but unlike in the tragedy of the commons, this strategy still exists and is used by bacteria. We discuss this evidence further in in section 2.3, and we also discuss this in the model analysis in chapter 5.
There are different mutations that can appear in *Pseudomonas aeruginosa* cells. As first there can appear signal-negative strains, which do not produce 3-oxo-C12-homoserine lactone autoinducers but still respond to signals. This mutant has the advantage that it does not produce autoinducers, but it still has the effort for the gene response. The second strain is called signal-blind strain, which does not respond to signals [27]. In the following we analyzed data with lasR rhlR mutants. These are double mutants that neither produce nor respond to quorum sensing signals [33]. We study how those lasR rhlR cheater cells exploit PA14 cells, based on theory and on data.

2.3. Evolutionary Stability of Quorum Sensing

In the section above we introduced the exploitation of the cooperative behavior in cells like *Pseudomonas aeruginosa* that use quorum sensing. The question arises, why quorum sensing is evolutionary stable, when cheating cells exploit the cooperative behavior. There have been found different explanations for this fact. At first, there can be a so called kin selection, where cheater cells cannot really exploit PA14 cells, since PA14 cells only share public goods with relatives. When cells are highly related, an exchange of products with cheater cells is much more likely than for a lower relatedness [12]. Moreover, there has been shown that cheating cells can get punished by PA14 cells with cyanide, since these cooperating PA14 cells were less susceptible to cyanide than the cheater cells [15]. It

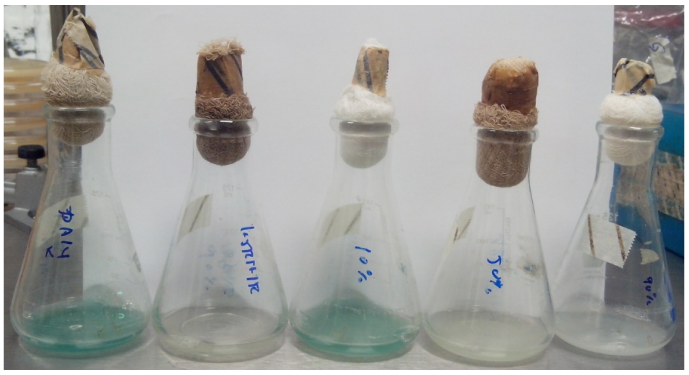

Figure 2.2.: Picture of the experimental setup. From left to right: PA14 (wildtype cells) lasR rhlR (cheater cells) 10% lasR rhlR 50% lasR rhlR 90% lasR rhlR.

has also been found that oxidative stress selects for cells with an active quorum sensing system, and reduces the amount of cheater cells [21]. Another interesting phenomenon is the mechanism of metabolic prudence. This mechanism takes care, that public-goods only get exchanged when it is most beneficial for the cooperating cells [14]. Spatial structuring of populations has also been shown to contribute to stability of cooperation [23].

2.4. Experimental Setup and Data Generation

In this section, we want to introduce the data we used for our analysis. We had different measurements of lasR rhlR mutants and PA14 cells growing together in different conditions, as depicted in figure 2.2. In the left vessel, PA14 cells were growing without lasR rhlR mutants for 24 hours. In the second vessel (from left), lasR rhlR mutants were growing without PA14 cells. In the other vessels, a mixture of $10\%, 50\%$ and 90% lasR rhlR mutants were growing together with PA14 cells. There were eleven measurement time-points (after hour $0, 2, 3, 4, 5, 6, 7, 8, 9, 10, 24$) where the cell density was measured for all of the five scenarios. The cell density was converted to the number of cells, which we used for our fitting procedures. Additionally, at 5 time-points (after hour $0, 4, 6, 10, 24$) the proportions of lasR rhlR and PA14 cells were measured. In García-Contreras et al. [21], there was already some similar work done on this topic. There, PA14 cells were growing alone, but social cheater cells could be detected after 48 hours. In our case, we already had a percentage of lasR rhlR cells growing with the PA14 cells at the beginning. We wanted to study the dynamics of lasR rhlR and PA14 cells depending on the starting conditions and were interested in exploring the interaction of both populations in all these cases. Therefore we used our modeling approaches and evaluated them afterwards.

3. Mathematical Background

In the following we start with mathematical basics and introduce notations that we follow throughout this thesis. We also present some models that are already well-known and that we adapt for the case we are studying.

3.1. Mathematical Models

Using standard tools (see for example Kuttler [3]), we consider a population where members are growing with a constant rate r and dying with a constant rate d. We define a function $x(t)$ describing the number of cells of a population x at time t. From now on we use the abbreviated form x. The rate of change of the population x over time t is written as $\frac{\mathrm{d}x}{\mathrm{d}t}$. Dividing the rate of change with the number of cells in the population $\frac{1}{x}\frac{\mathrm{d}x}{\mathrm{d}t}$ yields the per capita rate of change. We can define the intrinsic rate of growth $f = r - d$, which leaves us with the differential equation

$$\frac{1}{x}\frac{\mathrm{d}x}{\mathrm{d}t} = f.$$

Reformulation this equation we get:

$$\frac{\mathrm{d}x}{\mathrm{d}t} = fx. \tag{3.1}$$

With an initial condition $x(0) = k$, where k is the number of cells, we can get the explicit solution of this equation as $x(t) = ke^{ft}$, and we can distinguish three different cases. If $f > 0$, the population has an unlimited growth whereas for $f < 0$, the population decays exponentially. If $f = 0$, the population size is constant. We can directly see, that we cannot model bacterial growth with this model, since a bacterial population does typically not decay or grow exponentially. Bacterial populations do not grow unlimited, since there is always some competition for resources and space. As an improved model, we consider the deterministic logistic model in continuous time.

3.1.1. Logistic Model (Model 1)

The logistic model is a simple approach to model the growth of microorganisms, for example of bacteria. Instead of defining an intrinsic rate of growth, we now define the function $f(x) = r - dx$ being the difference of a growth rate r and a death function dx, where dx is increasing in the number of bacteria. This leads to the fact that the population does not grow unlimited. We can again formulate a differential equation

$$\frac{\mathrm{d}x}{\mathrm{d}t} = f(x)x, \quad f(x) = r - dx, \quad r > 0, \quad d > 0,$$

which can be reformulated as

$$\frac{\mathrm{d}x}{\mathrm{d}t} = f(x)x = (r - dx)x = rx(1 - \frac{dx}{r}).$$

Defining $d := \frac{r}{K}$, where K is referred to as the so called carrying capacity, we get

$$\frac{\mathrm{d}x}{\mathrm{d}t} = rx(1 - \frac{x}{K}). \tag{3.2}$$

For two populations x_1 and x_2 this reads

$$\frac{\mathrm{d}x_1}{\mathrm{d}t} = r_1 x_1(1 - \frac{x_1}{K_1}) \tag{3.3a}$$
$$\frac{\mathrm{d}x_2}{\mathrm{d}t} = r_2 x_2(1 - \frac{x_2}{K_2}). \tag{3.3b}$$

For populations growing independently of each other, the logistic model can be a good approach, but it is likely that models with an interaction term that accounts for competition between two populations are more appropriate to explain the dynamics of lasR rhlR mutants and wildtype cells growing together. In figure 3.1, a logistic growth curve of yeast in a sugar solution is depicted.

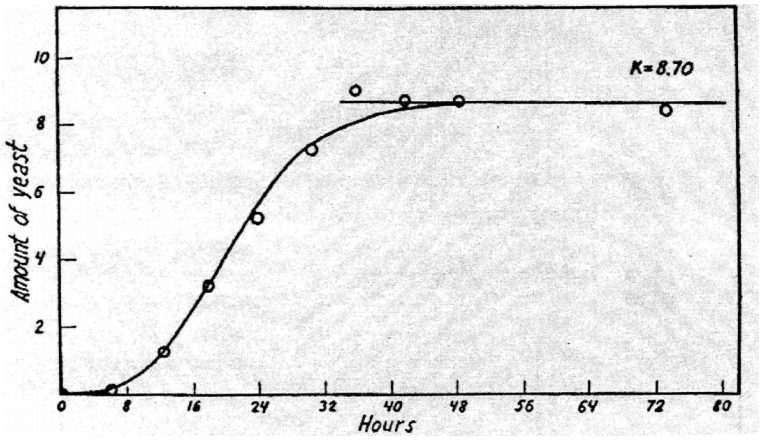

Figure 3.1.: Logistic growth curve of yeast in a sugar solution, with a carrying capacity K=8.70. The amount of yeast is depicted as a function of time. The picture is taken from Müller [9].

3.1.2. Competitive Lotka Volterra Model (Model 2)

The following model takes interaction among two populations into account. It can explain the dynamics of two populations that compete for example for nutrients and space. The model looks similar to the logistic model, but a new term is included, which accounts for the negative interaction (i. e. the presence of one population impacts the numbers of the other, denoted by the - term) between the two populations. It looks as follows (see Müller [9])

$$\frac{\mathrm{d}x_1}{\mathrm{d}t} = r_1 x_1 (1 - \frac{x_1 + \alpha_{12} x_2}{K_1}) \tag{3.4a}$$

$$\frac{\mathrm{d}x_2}{\mathrm{d}t} = r_2 x_2 (1 - \frac{x_2 + \alpha_{21} x_1}{K_2}). \tag{3.4b}$$

We can derive the model by defining f_1 and f_2 as functions that have an additional interaction term included representing the competition effect between the populations. The symbol α_{12} represents the negative effect that population x_2 has on population x_1 whereas the symbol α_{21} represents the negative effect that population x_1 has on population x_2. Defining $d_1 := \frac{r_1}{K_1}$ and $d_2 := \frac{r_2}{K_2}$ and setting

$$\frac{\mathrm{d}x_1}{\mathrm{d}t} = f_1(x_1, x_2) x_1 \tag{3.5a}$$

$$\frac{\mathrm{d}x_2}{\mathrm{d}t} = f_2(x_1, x_2) x_2 \tag{3.5b}$$

with

$$f_1(x_1, x_2) = r_1 - \alpha_{12} d_1 x_2 - d_1 x_1$$
$$f_2(x_1, x_2) = r_2 - \alpha_{21} d_2 x_1 - d_2 x_2,$$

we get the differential equations as introduced above. This model might be helpful to better explain the dynamics in our case, since the lasR rhlR mutants are likely to have a negative effect on the PA14 cells due to the exploitation of public goods. But this model might still not be sufficient, since in this case, a negative interaction between the populations is assumed. In our case however, there might not be a negative interaction term for the lasR rhlR mutants, they might rather profit from the appearance of PA14 cells. In chapter 4, we take this idea into account in our modeling approaches.

3.2. Tools for Stability Analysis

We want to analyze the behavior of the models we introduce. Therefore, we calculate the stationary points and additionally look at the behavior of the dynamical system near the stationary points. At first, we want to introduce some tools that we need for the stability analysis. Since we have nonlinear differential equations, we want to use a linearization to analyze the differential equations at the stationary points. Assume we have a two-dimensional system of differential equations with a stationary point $(\bar{x}, \bar{y})$ of $(f(x,y), g(x,y))^T = (\dot{x}, \dot{y})^T$, meaning that $(f(\bar{x}, \bar{y}), g(\bar{x}, \bar{y}))^T = (0,0)^T$. Consider a perturbation $x = \bar{x} + u, y = \bar{y} + v$, which yields (see Müller [9])

$$\dot{x} = (\bar{x} + u)^{\cdot} = f(\bar{x} + u, \bar{y} + v) = f(\bar{x}, \bar{y}) + \frac{\partial f(\bar{x}, \bar{y})}{\partial x} u + \frac{\partial f(\bar{x}, \bar{y})}{\partial y} v + ...$$
$$\dot{y} = (\bar{y} + v)^{\cdot} = g(\bar{x} + u, \bar{y} + v) = g(\bar{x}, \bar{y}) + \frac{\partial g(\bar{x}, \bar{y})}{\partial x} u + \frac{\partial g(\bar{x}, \bar{y})}{\partial y} v + ...$$

Near to the stationary point, we neglect higher order terms and find approximately

$$\dot{u} = \frac{\partial f}{\partial x} u + \frac{\partial f}{\partial y} v$$
$$\dot{v} = \frac{\partial g}{\partial x} u + \frac{\partial g}{\partial y} v.$$

In the following, we introduce two theorems that are helpful to analyze the behavior at the stationary points of a two-dimensional nonlinear differential equation.

Theorem 1 (Special case of Hartman-Grobman Theorem) *Let $(\bar{x}, \bar{y})$ be a stationary point, and let both eigenvalues λ of the Jacobian evaluated at the stationary point have*

a real part not equaling zero. Then all solution curves of the nonlinear system

$$\dot{x} = f(x, y)$$
$$\dot{y} = g(x, y)$$

show the same qualitative behaviour at the stationary point $(\bar{x}, \bar{y})$ *as those of the corresponding linear problem*

$$\begin{pmatrix} \dot{u} \\ \dot{v} \end{pmatrix} = \begin{pmatrix} \frac{\partial f}{\partial u} & \frac{\partial f}{\partial v} \\ \frac{\partial g}{\partial u} & \frac{\partial g}{\partial v} \end{pmatrix} \begin{pmatrix} u \\ v \end{pmatrix}.$$

Note that this theorem is only valid if both eigenvalues have a real part not equalling zero.

The Hartman-Grobman theorem and this special case can both be found in Müller [9].

Theorem 2 (Stability) *A stationary point* $(\bar{x}, \bar{y})$ *is stable if all of the eigenvalues of the Jacobian matrix evaluated at* $(\bar{x}, \bar{y})$ *have negative real parts. The stationary point is unstable if at least one of the eigenvalues has a positive real part.*

The proof of this theorem can be found in Arrowsmith [7].

3.3. Tools for Parameter Estimation

In the following, we explain the fitting procedure that we executed with MATLAB, show how we calculated the profile likelihoods for the best parameter vectors, and introduce the Akaike Information Criterion that is used for the model selection in chapter 5.

3.3.1. Fitting Procedure

We did parameter estimation for our models via the lsqnonlin method in MATLAB. The function lsqnonlin requires a function defined as

$$f(\theta) = \begin{pmatrix} f_1(\theta) \\ f_2(\theta) \\ \vdots \\ f_n(\theta) \end{pmatrix}$$

and then solves the nonlinear-least-squares curve fitting problem of the form

$$\min_{\theta} ||f(\theta)||_2^2 = \min_{\theta}(f_1(\theta)^2 + f_2(\theta)^2 + ... + f_n(\theta)^2),$$

in which optionally lower and upper bounds can be added on the components of θ. In our case, we wanted to find the best parameter vector $\hat{\theta} \in \mathbb{R}^m$ of a model with m parameters that minimizes a function dependent on the observed and estimated values of the model. The function which needs to be minimized is $\sum_{i=1}^{n}(y_{obs_i} - y_{pred_i}(\theta))^2$, and the minimization that is required to find the optimal vector $\hat{\theta} \in \mathbb{R}^m$ with the lsqnonlin method in MATLAB is therefore

$$\min_{\theta} ||E(\theta)||_2^2 = \min_{\theta} \sum_{i=1}^{n}(y_{obs_i} - y_{pred_i}(\theta))^2, \tag{3.6}$$

where y_{obs_i} denotes the ith observation in a time series of data, $y_{pred_i}(\theta)$ denotes a function of the parameter value which returns the predicted value of the ith observation. Therefore $E(\theta)$ has to be defined as

$$E(\theta) = \begin{pmatrix} (y_{obs_1} - y_{pred_1}(\theta)) \\ (y_{obs_2} - y_{pred_2}(\theta)) \\ \vdots \\ (y_{obs_n} - y_{pred_n}(\theta)) \end{pmatrix}.$$

We used a random number generator that calculated a starting vector $\theta \in \mathbb{R}^m$ and run the lsqnonlin fitting procedure for numerous starting vectors, since the lsqnonlin method only finds local minima. The used algorithm is called trust-region-reflective algorithm, and is based on the interior-reflective Newton method [32].

3.3.2. Profile Likelihood Calculation

Later we want to check if there is evidence that some of the parameters of the best parameter vector $\hat{\theta}$ are not identifiable. We can use the profile likelihood method to give evidence for a non-identifiable parameter. Under normally distributed measurement noise, we get the log-likelihood as

$$\log(L(\theta)) = -\frac{n}{2}\log(2\pi\sigma) - \frac{\sum_{i=1}^{n}(y_{obs_i} - y_{pred_i}(\theta))^2}{2\sigma},$$

where $\sigma = \frac{1}{n-1}\sum_{i=1}^{n}(y_{obs_i} - y_{pred_i}(\theta))^2$ denotes the sample variance. The profile likelihood $PL(\theta_i)$ for parameter θ_i can be derived as

$$PL(\theta_i) = \min_{\theta_{j\neq i}} L(\theta), \tag{3.7}$$

where θ_i is fixed, and where we minimize over $\theta_{j\neq i}$. To calculate a confidence interval I of the parameters θ_i to a significance level α, we calculate

$$I(\theta_i) = \{\theta_i | P(\theta_i) - L(\hat{\theta}) < \eta_\alpha\}, \tag{3.8}$$

where $\eta_\alpha = (\chi^2)^{-1}(\theta_n \leq \alpha, 1)/2$ can be calculated via the chi-squared inverse cumulative distribution function. In Raue et al. [1], the procedure is explained in more detail.

3.3.3. Akaike Information Criterion

After we find the optimal parameter values for the models, we use the Akaike Information Criterion (AIC) to evaluate the relative quality of our models. The AIC value can be calculated via the formula

$$AIC = 2k - 2\log(L(\hat{\theta})), \tag{3.9}$$

where $L(\hat{\theta})$ denotes the maximized value of the likelihood function and k the number of parameters in the model. We can evaluate the goodness of fit of our models with the AIC value. It takes the number of parameters into account in the form of a penalty for the number of parameters. Therefore, we can compare the introduced models, although they do not all have the same number of parameters. The smaller the AIC value, the better the model fits the data [8].

4. Modeling

Here we want to show different modeling approaches that we used to analyze the data. We mainly base the modeling approaches on biological theory and use ideas of the models introduced in chapter 3. To remind the reader, the wildtype produces public goods which they use but also the cheaters take advantage of, without producing them. Producing these goods is costly (energy-wise) for the wildtype. We present modeling approaches with a profit term included in the growth rate of PA14 cells (x_1) and the lasR rhlR mutants (x_2). In Brown et al. [26], approaches with a benefit for both populations of the public goods produced by the PA14 cells and an included cost term for the PA14 cells were presented. We do not explicitly model a cost term for the PA14 cells for producing those public goods. In our models this cost term is included in the independent part of the growth rate of the wildtype cells indirectly.
In section 4.2., we present models that have an interaction term included, as seen for the Competitive Lotka Volterra model.

4.1. Logistic Models with Growth Benefit

The following models have a profit term included in their growth rates. This is motivated by the finding that there is a profit for lasR rhlR mutants that exploit the PA14 wildtype cells, and there is also an effect on the growth rate for PA14 cells dependent on the amount of lasR rhlR mutants.

4.1.1. Growth Benefit for Both Populations (Model 3)

The following model has an interaction term included in the growth rate of both populations which is dependent on the proportion of population x_1 and population x_2. We split the growth rates of the two populations in two parts. At first we have a part being independent of the other population (r_1 for population x_1 and r_2 for population x_2) and secondly a part being dependent on the other population ($\frac{p_1 x_2}{x_1+x_2}$ for population x_1 and $\frac{p_2 x_1}{x_1+x_2}$ for population x_2). We define

$$\frac{\mathrm{d}x_1}{\mathrm{d}t} = f_1(x_1, x_2)x_1, \quad f_1(x_1, x_2) = (r_1 + \frac{p_1 x_2}{x_1 + x_2}) - d_1 x_1, \quad d_1 > 0 \tag{4.1a}$$

$$\frac{\mathrm{d}x_2}{\mathrm{d}t} = f_2(x_1, x_2)x_2, \quad f_2(x_1, x_2) = (r_2 + \frac{p_2 x_1}{x_1 + x_2}) - d_2 x_2, \quad d_2 > 0, \tag{4.1b}$$

with growth functions $\tilde{r_1}(x_1, x_2) = r_1 + \frac{p_1 x_2}{x_1 + x_2}$ for equation (4.1a) and $\tilde{r_2}(x_1, x_2) = r_2 + \frac{p_2 x_1}{x_1 + x_2}$ for equation (4.1b). Rewriting $d_1 := \frac{\tilde{r_1}(x_1, x_2)}{K_1}$ and $d_2 := \frac{\tilde{r_2}(x_1, x_2)}{K_2}$, we get for population x_1

$$\begin{aligned}
\frac{\mathrm{d}x_1}{\mathrm{d}t} &= (\tilde{r_1}(x_1, x_2) - d_1 x_1)x_1 \\
&= x_1(\tilde{r_1}(x_1, x_2) - \frac{\tilde{r_1}(x_1, x_2)x_1}{K_1}) \\
&= \tilde{r_1}(x_1, x_2)x_1(1 - \frac{x_1}{K_1})
\end{aligned}$$

and for population x_2

$$\begin{aligned}
\frac{\mathrm{d}x_2}{\mathrm{d}t} &= (\tilde{r_2}(x_1, x_2) - d_2 x_2)x_2 \\
&= x_2(\tilde{r_2}(x_1, x_2) - \frac{\tilde{r_2}(x_1, x_2)x_2}{K_2}) \\
&= \tilde{r_2}(x_1, x_2)x_2(1 - \frac{x_2}{K_2}).
\end{aligned}$$

Thus, we end up with the following system of differential equations

$$\frac{\mathrm{d}x_1}{\mathrm{d}t} = (r_1 + p_1 \frac{x_2}{x_1 + x_2})x_1(1 - \frac{x_1}{K_1}) \tag{4.2a}$$

$$\frac{\mathrm{d}x_2}{\mathrm{d}t} = (r_2 + p_2 \frac{x_1}{x_1 + x_2})x_2(1 - \frac{x_2}{K_2}), \tag{4.2b}$$

where x_1 represents the population of PA14 cells, and x_2 the population of lasR rhlR cells.

4.1.2. Growth Benefit for One Population (Model 4)

In this model (Model 4 (i)), the PA14 cells profit from the lasR rhlR mutants in form of a higher growth rate, depending on the proportions of cheaters. We define

$$\frac{\mathrm{d}x_1}{\mathrm{d}t} = f_1(x_1, x_2)x_1, \quad f_1(x_1, x_2) = (r_1 + \frac{p_1 x_2}{x_1 + x_2}) - d_1 x_1, \quad d_1 > 0 \tag{4.3a}$$

$$\frac{\mathrm{d}x_2}{\mathrm{d}t} = f_2(x_1, x_2)x_2, \quad f_2(x_1, x_2) = r_2 - d_2 x_2, \quad d_2 > 0, \tag{4.3b}$$

with growth function $\tilde{r_1}(x_1, x_2) = r_1 + \frac{p_1 x_2}{x_1 + x_2}$ for equation (4.3a) and growth rate r_2 for equation (4.3b). Setting $d_1 := \frac{\tilde{r_1}(x_1, x_2)}{K_1}$ and $d_2 := \frac{r_2}{K_2}$, we get the according system of differential equations after similar computations as

$$\frac{\mathrm{d}x_1}{\mathrm{d}t} = (r_1 + p_1 \frac{x_2}{x_1 + x_2})x_1(1 - \frac{x_1}{K_1}) \tag{4.4a}$$

$$\frac{\mathrm{d}x_2}{\mathrm{d}t} = r_2 x_2(1 - \frac{x_2}{K_2}), \tag{4.4b}$$

where x_1 represent the PA14 cells, and x_2 the lasR rhlR mutants.
The following Model 4 (ii) accounts for the fact that the growth benefit for PA14 cells might be rather low, possibly even negative, and that rather the lasR rhlR mutant has a growth benefit of the PA14 cells than the opposite case. The formula can be derived analogously and reads

$$\frac{\mathrm{d}x_1}{\mathrm{d}t} = r_1 x_1(1 - \frac{x_1}{K_1}) \tag{4.5a}$$

$$\frac{\mathrm{d}x_2}{\mathrm{d}t} = (r_2 + p_2 \frac{x_1}{x_1 + x_2})x_2(1 - \frac{x_2}{K_2}), \tag{4.5b}$$

with the PA14 cells x_1 and lasR rhlR cells x_2.

4.2. Logistic Models with Growth Benefit and Interaction

In this section we combine ideas of the models introduced above. We include concepts from the Competitive Lotka Volterra Model as well as a growth benefit as introduced in section 4.1. We use an interaction term for the interaction of lasR rhlR mutants with PA14 cells and vice versa, and additionally, we include a profit term in the growth rates for the two cell types.

4.2.1. Negative Interaction with Growth Benefit for Both Populations (Model 5)

This model has an interaction term similar to the Competitive Lotka Volterra model (Model 2), but an additional profit term included in the growth term. In this model we assume that also PA14 cells may have some benefit from lasR rhlR mutants. We define

$$\frac{\mathrm{d}x_1}{\mathrm{d}t} = f_1(x_1, x_2)x_1 \tag{4.6a}$$
$$\frac{\mathrm{d}x_2}{\mathrm{d}t} = f_2(x_1, x_2)x_2, \tag{4.6b}$$

with

$$f_1(x_1, x_2) = (r_1 + \frac{p_1 x_2}{x_1 + x_2}) - \alpha_{12} d_1 x_2 - d_1 x_1$$
$$f_2(x_1, x_2) = (r_2 + \frac{p_2 x_1}{x_1 + x_2}) - \alpha_{21} d_2 x_1 - d_2 x_2,$$

such that we can formulate the system of differential equations as

$$\frac{\mathrm{d}x_1}{\mathrm{d}t} = \left[(r_1 + \frac{p_1 x_2}{x_1 + x_2}) - \alpha_{12} d_1 x_2 - d_1 x_1\right] x_1 \tag{4.7a}$$
$$\frac{\mathrm{d}x_2}{\mathrm{d}t} = \left[(r_2 + \frac{p_2 x_1}{x_1 + x_2}) - \alpha_{21} d_2 x_1 - d_2 x_2\right] x_2. \tag{4.7b}$$

As before, we have growth functions $\tilde{r_1}(x_1, x_2) = r_1 + \frac{p_1 x_2}{x_1 + x_2}$ and $\tilde{r_2}(x_1, x_2) = r_2 + \frac{p_2 x_1}{x_1 + x_2}$. Reformulating for x_1 with $d_1 := \frac{\tilde{r_1}(x_1, x_2)}{K_1}$ and x_2 with $d_2 := \frac{\tilde{r_2}(x_1, x_2)}{K_2}$, we get

$$\frac{\mathrm{d}x_1}{\mathrm{d}t} = (r_1 + p_1 \frac{x_2}{x_1 + x_2}) x_1 (1 - \frac{x_1 + \alpha_{12} x_2}{K_1}) \tag{4.8a}$$
$$\frac{\mathrm{d}x_2}{\mathrm{d}t} = (r_2 + p_2 \frac{x_1}{x_1 + x_2}) x_2 (1 - \frac{x_2 + \alpha_{21} x_1}{K_2}). \tag{4.8b}$$

4.2.2. Negative Interaction Model with Growth Benefit for One Population (Model 6)

The following model is very similar to Model 5, but has one parameter less. It has only a profit term for the lasR rhlR cells included, which might be a more realistic scenario. We get

$$\frac{\mathrm{d}x_1}{\mathrm{d}t} = f_1(x_1, x_2)x_1$$
$$\frac{\mathrm{d}x_2}{\mathrm{d}t} = f_2(x_1, x_2)x_2$$

with f_1 and f_2 defined as

$$f_1(x_1, x_2) = r_1 - \alpha_{12}d_1x_2 - d_1x_1$$

$$f_2(x_1, x_2) = (r_2 + \frac{p_2x_1}{x_1 + x_2}) - \alpha_{21}d_2x_1 - d_2x_2.$$

After a similar procedure in deriving the differential equations, we end up with the model

$$\frac{\mathrm{d}x_1}{\mathrm{d}t} = r_1x_1(1 - \frac{x_1 + \alpha_{12}x_2}{K_1}) \tag{4.9a}$$
$$\frac{\mathrm{d}x_2}{\mathrm{d}t} = (r_2 + p_2\frac{x_1}{x_1 + x_2})x_2(1 - \frac{x_2 + \alpha_{21}x_1}{K_2}). \tag{4.9b}$$

4.2.3. Positive Interaction Model (Model 7)

We now consider again a modeling approach, where PA14 cells get punished from the lasR rhlR mutants. In this approach, the growth rate of the PA14 cells is not directly influenced by the proportions of lasR rhlR mutants. For the lasR rhlR cells, we take a positive interaction term instead of a negative one, accounting for the fact, that the interaction with the PA14 mutants has a positive effect on the lasR rhlR mutants instead of a negative effect as it is the case for the Competitive Lotka Volterra model. We get

$$\frac{\mathrm{d}x_1}{\mathrm{d}t} = f_1(x_1, x_2)x_1$$
$$\frac{\mathrm{d}x_2}{\mathrm{d}t} = f_2(x_1, x_2)x_2$$

with f_1 and f_2 defined as

$$f_1(x_1, x_2) = r_1 - \alpha_{12}d_1x_2 - d_1x_1$$
$$f_2(x_1, x_2) = r_2 + \alpha_{21}d_2x_1 - d_2x_2.$$

For the PA14 cells we end up with the Competitive Lotka Volterra Model as introduced before. After reformulating the equations with $d_1 := \frac{r_1}{K_1}$ and $d_2 := \frac{r_2}{K_2}$ we get

$$\frac{\mathrm{d}x_1}{\mathrm{d}t} = r_1 x_1 (1 - \frac{x_1 + \alpha_{12} x_2}{K_1}) \tag{4.10a}$$
$$\frac{\mathrm{d}x_2}{\mathrm{d}t} = r_2 x_2 (1 - \frac{x_2 - \alpha_{21} x_1}{K_2}), \tag{4.10b}$$

where x_1 describes the PA14 cells and where x_2 describes the lasR rhlR mutants.

4.2.4. Positive Interaction Model with Growth Benefit (Model 8)

In this model, we use the idea of a positive interaction for lasR rhlR mutants with PA14 cells, that additionally have a positive interaction with the PA14 cells in the growth rate included. For the PA14 cells, we assume a negative interaction with the lasR rhlR mutants as seen for the Competitive Lotka Volterra model. We get

$$\frac{\mathrm{d}x_1}{\mathrm{d}t} = f_1(x_1, x_2) x_1$$
$$\frac{\mathrm{d}x_2}{\mathrm{d}t} = f_2(x_1, x_2) x_2$$

with f_1 and f_2 defined as

$$f_1(x_1, x_2) = r_1 - \alpha_{12} d_1 x_2 - d_1 x_1$$

$$f_2(x_1, x_2) = (r_2 + \frac{p_2 x_1}{x_1 + x_2}) + \alpha_{21} d_2 x_1 - d_2 x_2,$$

resulting in

$$\frac{\mathrm{d}x_1}{\mathrm{d}t} = (r_1 - \alpha_{12} d_1 x_2 - d_1 x_1) x_1 \tag{4.11a}$$
$$\frac{\mathrm{d}x_2}{\mathrm{d}t} = ((r_2 + \frac{p_2 x_1}{x_1 + x_2}) + \alpha_{21} d_2 x_1 - d_2 x_2) x_2. \tag{4.11b}$$

After very similar derivations we end up with the equations

$$\frac{\mathrm{d}x_1}{\mathrm{d}t} = r_1 x_1 (1 - \frac{x_1 + \alpha_{12} x_2}{K_1}) \tag{4.12a}$$
$$\frac{\mathrm{d}x_2}{\mathrm{d}t} = (r_2 + p_2 \frac{x_1}{x_1 + x_2}) x_2 (1 - \frac{x_2 - \alpha_{21} x_1}{K_2}), \tag{4.12b}$$

where x_1 represents the PA14 cells and x_2 represents the lasR rhlR mutants.

4.2.5. Symmetrical Approach with Growth Benefit and Negative Interaction (Model 9)

Here we want to present a symmetrical modeling approach. PA14 cells also profit from their own produced public goods. If the proportion of PA14 cells is high, the PA14 cells should be able to use a higher percentage of public goods. We get

$$\frac{\mathrm{d}x_1}{\mathrm{d}t} = f_1(x_1, x_2) x_1$$
$$\frac{\mathrm{d}x_2}{\mathrm{d}t} = f_2(x_1, x_2) x_2$$

with f_1 and f_2 defined as

$$f_1(x_1, x_2) = (r_1 + \frac{p_1 x_1}{x_1 + x_2}) - \alpha_{12} d_1 x_2 - d_1 x_1$$

$$f_2(x_1, x_2) = (r_2 + \frac{p_2 x_1}{x_1 + x_2}) - \alpha_{21} d_2 x_1 - d_2 x_2,$$

resulting in

$$\frac{\mathrm{d}x_1}{\mathrm{d}t} = (r_1 + \frac{p_1 x_1}{x_1 + x_2}) - \alpha_{12} d_1 x_2 - d_1 x_1) x_1 \tag{4.13a}$$
$$\frac{\mathrm{d}x_2}{\mathrm{d}t} = ((r_2 + \frac{p_2 x_1}{x_1 + x_2}) - \alpha_{21} d_2 x_1 - d_2 x_2) x_2. \tag{4.13b}$$

After rewriting $d_1 = \frac{r_1(\tilde{x_1},x_2)}{K_1}$ and $d_2 = \frac{r_2(\tilde{x_1},x_2)}{K_2}$ with $\tilde{r_1}(x_1,x_2) = r_1 + \frac{p_1 x_1}{x_1+x_2}$ and $\tilde{r_2}(x_1,x_2) = r_2 + \frac{p_2 x_1}{x_1+x_2}$ and reformulating, we get

$$\frac{\mathrm{d}x_1}{\mathrm{d}t} = (r_1 + p_1\frac{x_1}{x_1+x_2})x_1(1 - \frac{x_1+\alpha_{12}x_2}{K_1}) \tag{4.14a}$$
$$\frac{\mathrm{d}x_2}{\mathrm{d}t} = (r_2 + p_2\frac{x_1}{x_1+x_2})x_2(1 - \frac{x_2+\alpha_{21}x_1}{K_2}). \tag{4.14b}$$

4.2.6. Symmetrical Approach with Growth Benefit and Positive Interaction (Model 10)

Here we again model slightly different, instead of having a negative interaction term for lasR rhlR mutants, we take a positive interaction term, that accounts for a positive influence of wildtype cells on lasR rhlR mutants. A profit term for both populations by the public goods production is again included, and a negative interaction term for the wildtype cells with the lasR rhlR mutants. We get

$$\frac{\mathrm{d}x_1}{\mathrm{d}t} = f_1(x_1,x_2)x_1$$
$$\frac{\mathrm{d}x_2}{\mathrm{d}t} = f_2(x_1,x_2)x_2$$

with f_1 and f_2 defined as

$$f_1(x_1,x_2) = (r_1 + \frac{p_1 x_1}{x_1+x_2}) - \alpha_{12}d_1x_2 - d_1x_1$$

$$f_2(x_1,x_2) = (r_2 + \frac{p_2 x_1}{x_1+x_2}) + \alpha_{21}d_2x_1 - d_2x_2,$$

which gives

$$\frac{\mathrm{d}x_1}{\mathrm{d}t} = ((r_1 + \frac{p_1 x_1}{x_1+x_2}) - \alpha_{12}d_1x_2 - d_1x_1)x_1 \tag{4.15a}$$
$$\frac{\mathrm{d}x_2}{\mathrm{d}t} = ((r_2 + \frac{p_2 x_1}{x_1+x_2}) + \alpha_{21}d_2x_1 - d_2x_2)x_2. \tag{4.15b}$$

After rewriting $d_1 = \frac{r_1(\tilde{x_1},x_2)}{K_1}$ and $d_2 = \frac{r_2(\tilde{x_1},x_2)}{K_2}$ with $\tilde{r_1}(x_1,x_2) = r_1 + \frac{p_1 x_1}{x_1+x_2}$ and $\tilde{r_2}(x_1,x_2) = r_2 + \frac{p_2 x_1}{x_1+x_2}$, we get

$$\frac{\mathrm{d}x_1}{\mathrm{d}t} = (r_1 + p_1\frac{x_1}{x_1+x_2})x_1(1 - \frac{x_1+\alpha_{12}x_2}{K_1}) \tag{4.16a}$$

$$\frac{\mathrm{d}x_2}{\mathrm{d}t} = (r_2 + p_2\frac{x_1}{x_1+x_2})x_2(1 - \frac{x_2-\alpha_{21}x_1}{K_2}), \tag{4.16b}$$

where x_1 describes the PA14 cells and x_2 describes the lasR rhlR mutants.

4.3. Summary of Model Properties

In this section, we want to sum up the models we introduced in the previous sections. We list the properties of the different models in a table, to have a better overview (see figure 4.1.).

Properties	g.t. x_1	g.t. x_2	i.t. x_1	i.t. x_2
Model 1	−	−	−	−
Model 2	−	−	+	+
Model 3	+	+	−	−
Model 4(i)	+	−	−	−
Model 4(ii)	−	+	−	−
Model 5	+	+	+	+
Model 6	−	+	+	+
Model 7	−	−	+	+
Model 8	−	+	+	+
Model 9	+	+	+	−
Model 10	+	+	+	+

Figure 4.1.: Depicted are the different properties of the models. g.t. means growth term, i.t. means interaction term. As an example, g.t. x_1 means that a growth term is included in the differential equation of x_1. A minus means, that the specific model does not include this property, whereas a plus means, that the model has this property.

5. Model Analysis

In the following, we perform a stability analysis for the logistic model and for the Competitive Lotka Volterra model. For the other models we introduced above we list the stationary points.

5.1. Stability Analysis

5.1.1. Logistic Model

To calculate the stationary points, both equations are set to zero. It follows

$$\frac{\mathrm{d}x_1}{\mathrm{d}t} = r_1 x_1 (1 - \frac{x_1}{K_1}) = 0 \Leftrightarrow x_1 \in \{0, K_1\}$$

$$\frac{\mathrm{d}x_2}{\mathrm{d}t} = r_2 x_2 (1 - \frac{x_2}{K_2}) = 0 \Leftrightarrow x_2 \in \{0, K_2\}.$$

Thus, we get the four stationary points

$$P_1 = (0,0), \quad P_2 = (0,K_2), \quad P_3 = (K_1,0), \quad P_4 = (K_1,K_2).$$

According to theorem 1, the nonlinear dynamical system has the same qualitative behavior at the stationary points as the according linear system. We calculate the Jacobian resulting in

$$J(x_1,x_2) = \begin{pmatrix} r_1 - \frac{2r_1x_1}{K_1} & 0 \\ 0 & r_2 - \frac{2r_2x_2}{K_2} \end{pmatrix}. \tag{5.1}$$

Now, we evaluate the Jacobian at the stationary points. For $P_1 = (0, 0)$, we get

$$J(0,0) = \begin{pmatrix} r_1 & 0 \\ 0 & r_2 \end{pmatrix}, \tag{5.2}$$

with eigenvalues $\lambda_1 = r_1$ and $\lambda_2 = r_2$. Since we assume that $r_1 > 0$ and $r_2 > 0$, the eigenvalues both are positive, and thus the point $P_1 = (0, 0)$ is unstable. We can now check for the second one. We have $P_2 = (0, K_2)$, inserting this in the Jacobian we get

$$J(0,K_2) = \begin{pmatrix} r_1 & 0 \\ 0 & -r_2 \end{pmatrix}, \tag{5.3}$$

with the eigenvalues $\lambda_1 = r_1$ and $\lambda_2 = -r_2$. We have again an unstable point, since one of the two eigenvalues is positive.
For the third point $P_3 = (K_1, 0)$, we get

$$J(K_1,0) = \begin{pmatrix} -r_1 & 0 \\ 0 & r_2 \end{pmatrix}, \tag{5.4}$$

again with the result, that one eigenvalue is positive and the other negative, resulting in an unstable point.
As the last point to check, $P_4 = (K_1, K_2)$, we get the resulting Jacobian as

$$J(K_1,K_2) = \begin{pmatrix} -r_1 & 0 \\ 0 & -r_2 \end{pmatrix}, \tag{5.5}$$

meaning that this point is a stable point, since $\lambda_1 = -r_1$ and $\lambda_2 = -r_2$ both are negative. In figure 5.1 the four stationary points are depicted.

5.1.2. Competitive Lotka Volterra Equations

Recall the model as

$$\frac{\mathrm{d}x_1}{\mathrm{d}t} = r_1 x_1 (1 - \frac{x_1 + \alpha_{12} x_2}{K_1}) \tag{5.6a}$$

$$\frac{\mathrm{d}x_2}{\mathrm{d}t} = r_2 x_2 (1 - \frac{x_2 + \alpha_{21} x_1}{K_2}). \tag{5.6b}$$

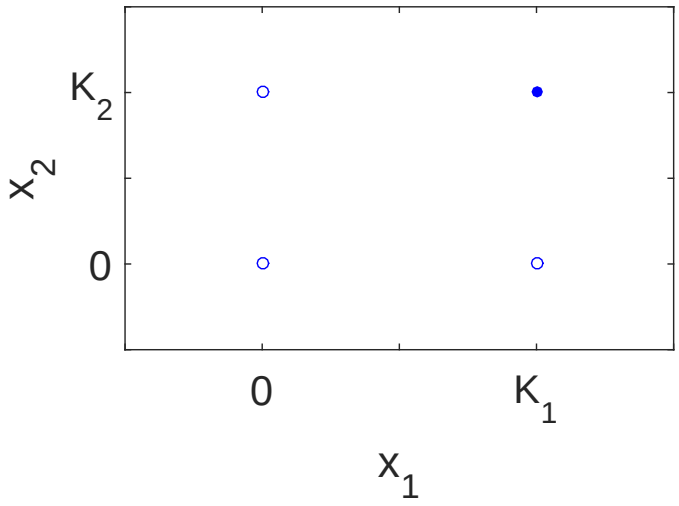

Figure 5.1.: Stationary points of the logistic model. The filled dot indicates the stable point, the unfilled dots indicate the unstable points.

We do the analysis according to Müller [9]. We can simplify the model with the definitions

$$y_1 := \frac{x_1}{K_1}, \quad y_2 := \frac{x_2}{K_2}, \quad \tau = r_1 t, \quad \rho := \frac{r_2}{r_1}, a_1 := \alpha_{12}\frac{K_2}{K_1}, \quad a_2 := \alpha_{21}\frac{K_1}{K_2}$$

and end up with the equations

$$\frac{\mathrm{d}y_1}{\mathrm{d}\tau} = y_1(1 - y_1 - a_1 y_2) \tag{5.7a}$$

$$\frac{\mathrm{d}y_2}{\mathrm{d}\tau} = \rho y_2(1 - y_2 - a_2 y_1). \tag{5.7b}$$

The stationary points can be calculated as

$$P_1 := (0,0), \quad P_2 := (1,0), \quad P_3 := (0,1), \quad P_4 := (\tfrac{a_1-1}{a_1a_2-1}, \quad \tfrac{a_2-1}{a_1a_2-1}),$$

and the Jacobian reads

$$J(y_1, y_2) = \begin{pmatrix} 1 - 2y_1 - a_1 y_2 & -a_1 y_1 \\ -\rho a_2 y_2 & \rho(1 - 2y_2 - a_2 y_1) \end{pmatrix}. \tag{5.8}$$

There are four different cases to consider for the stability analysis:
Case 1: $a_1 < 1$ and $1 < a_2$. We get the stationary points $P_1 = (0,0), \quad P_2 = (0,1), \quad P_3 = (1,0)$. The Jacobian matrix in $P_1 = (0,0)$ reads

$$J(0,0) = \begin{pmatrix} 1 & 0 \\ 0 & \rho \end{pmatrix}. \tag{5.9}$$

Thus, $P_1 = (0,0)$ is an unstable point, cause the eigenvalues both are positive. Note that ρ is positive, since we were assuming our growth rates to be positive.
For the second point $P_2 = (0,1)$, we get

$$J(0,1) = \begin{pmatrix} 1-a_1 & 0 \\ -\rho a_2 & -\rho \end{pmatrix}. \tag{5.10}$$

Thus, this point is an unstable point, since there is a positive and a negative eigenvalue.
For the third point, $P_3 = (1,0)$, we get the Jacobian as

$$J(1,0) = \begin{pmatrix} -1 & -a_1 \\ 0 & \rho(1-a_2) \end{pmatrix}. \tag{5.11}$$

Because of the assumption that $a_2 > 1$, the term $\rho(1-a_2)$ is negative, and thus both eigenvalues are negative, resulting in a stable point.
As a result, the population does not coexist, but y_2 takes over where y_1 dies out. We have the condition

$$a_1 = \alpha_{12}\frac{K_2}{K_1} < 1 < \alpha_{21}\frac{K_1}{K_2} = a_2, \tag{5.12}$$

thus either K_1 is larger than K_2 or α_{12} is much higher than α_{21}.

Case 2: $a_1 > 1$ and $a_2 < 1$. This case is similar to case 1, only that y_1 and y_2 switch their roles.

Case 3: $a_1, a_2 < 1$. In this case, a coexistence point is present. Thus, we have four stationary points, and we get the Jacobian of $(0,0)$ as

$$J(0,0) = \begin{pmatrix} 1 & 0 \\ 0 & \rho \end{pmatrix}. \tag{5.13}$$

We see that $(0,0)$ is unstable. For $(0,1)$, we get

$$J(0,1) = \begin{pmatrix} 1-a_1 & 0 \\ -\rho a_2 & -\rho \end{pmatrix}, \tag{5.14}$$

which is also an unstable point since we find a positive and a negative eigenvalue. For $(1,0)$ we get

$$J(1,0) = \begin{pmatrix} -1 & -a_1 \\ 0 & \rho(1-a_2) \end{pmatrix}. \tag{5.15}$$

We find a positive and a negative eigenvalue, leading to an unstable point. Calculating the characteristic polynomial for the fourth point $(\frac{a_1-1}{a_1a_2-1}, \frac{a_2-1}{a_1a_2-1})$, we find that this point is a stable point.
Case 4: $a_1, a_2 > 1$. Doing similar calculations as in case 3, we find that $(0,0)$ and $(\frac{a_1-1}{a_1a_2-1}, \frac{a_2-1}{a_1a_2-1})$ are unstable, whereas $(1,0), (0,1)$ are stable points.
Depending on the initial condition, one of the two species dies out, such that there will not be a coexistence.
Summing up, case 3 is the only case where both species coexist. The condition for case 3 to happen is

$$a_1 = \alpha_{12}\frac{K_2}{K_1} < 1, \quad \alpha_{21}\frac{K_1}{K_2} = a_2 < 1. \tag{5.16}$$

That this case happens, α_{12} and α_{21} must not be too large, since the upper inequalities have to hold. This means that a coexistence only happens when the interaction between the two populations is small. For the case that the interaction is high, only one species will survive on a continuing basis.
As we saw, it is already challenging to perform a stability analysis for this model. Since stability analysis is not the main focus of this work, we do not perform a stability analysis for the other models, however, we list the stationary points in the appendix.

5.2. Model Fitting and Parameter Estimation

In the following, we show the results of the parameter estimation with the models we introduced. The lasR rhlR mutants and PA14 cells were growing for twenty-four hours, and we had eleven measurement points (after hour $0, 2, 3, 4, 5, 6, 7, 8, 9, 10, 24$) where the

cell density was measured, and which we converted to the number of cells for our fitting procedure. Additionally, at five time-points (after hour $0, 4, 6, 10, 24$), the proportion of lasR rhlR cells and wildtype cells PA14 was measured, which we also converted to cell numbers for the fitting procedure. Altogether, we had 16 measurement points for our optimization. There were five different starting conditions. The first two conditions were lasR rhlR mutants and PA14 cells growing alone for twenty-four hours. The other conditions were the cases where 10%, 50% and 90% lasR rhlR mutants were growing together with PA14 cells. The scenario where only lasR rhlR mutants and PA14 cells were growing on their own are analyzed with the logistic model. These cases do not help in investigating the interactions between lasR rhlR mutants and PA14 cells. We also analyze the other scenarios with the logistic model, and look if we find some coherence between the different cases, according to the estimated values by the optimization with the logistic model. For the 10%, 50% and 90% we compare the models from chapter 3 and chapter 4 with the AIC.

5.2.1. Logistic Model Analysis

Before analyzing and evaluating the models in detail, we want to have a look at the logistic model, and see if there is some coherence between the different conditions that we study. It can help to see common properties shared among the cases, and help to evaluate and interpret the other models. This model assumes that two populations grow independently from each other (which is essentially not the case for PA14 and lasR rhlR mutants growing together). We fit each case (0%, 10%, 50%, 90% and 100% cheater), and look at the optimal parameter vectors of the fitting procedure. Recall the logistic model as

$$\frac{\mathrm{d}x}{\mathrm{d}t} = rx(1 - \frac{x}{K}). \tag{5.17}$$

We find for the cases where only lasR rhlR mutants and PA14 cells were growing alone, that lasR rhlR mutants grow less quickly than PA14 cells, and that the carrying capacity for the lasR rhlR mutants is lower than the carrying capacity of the PA14 cells. As best parameter values, we found the values $(\hat{r}, \hat{K}) = (0.45, 2.41 \times 10^7)$ for the PA14 cells, and $(\hat{r}, \hat{K}) = (0.13, 1.96 \times 10^6)$ for the lasR rhlR mutants. In figure 5.2 we see the two different growth curves of PA14 and lasR rhlR cells.

Now we want to study the scenarios where 10%, 50% and 90% lasR rhlR mutants were

Figure 5.2.(a)

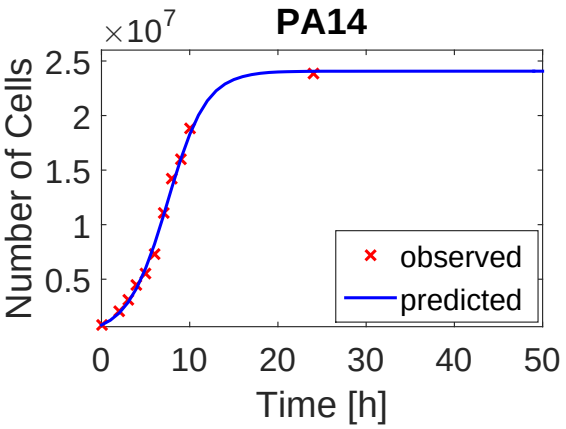

Figure 5.2.(b)

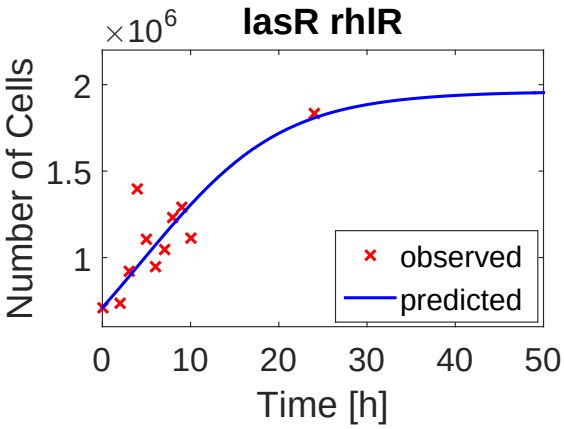

Figure 5.2.: Depicted are the fits for the logistic model (equation 5.17). The data points are shown as red crosses, whereas the fit is a blue line. The eleven data points are the average values of six different measurements (after hour $0, 2, 3, 4, 5, 6, 7, 8, 9, 10, 24$) where cell density got measured and was converted to the number of cells. The number of cells is plotted as a function of time. In figure 5.2.(a) we see the fit where only PA14 cells were growing, in figure 5.2.(b) we see the fit where only lasR rhlR mutants were growing.

growing at the beginning. Recall the logistic model as

$$\frac{\mathrm{d}x_1}{\mathrm{d}t} = r_1 x_1 (1 - \frac{x_1}{K_1}) \tag{5.18a}$$

$$\frac{\mathrm{d}x_2}{\mathrm{d}t} = r_2 x_2 (1 - \frac{x_2}{K_2}). \tag{5.18b}$$

10% lasR rhlR. We get the estimated vector $P = (\hat{r_1}, \hat{K_1}, \hat{r_2}, \hat{K_2}) = (0.37, 10.97 \times 10^7, 0.48, 10.66 \times 10^7)$. We can see that the growth rate $\hat{r_1}$ of the PA14 cells is now lower whereas the growth rate $\hat{r_2}$ of the lasR rhlR mutants is higher compared to the case where only lasR rhlR mutants and PA14 cells were growing alone, and even higher as the growth rate of PA14 cells. The carrying capacity is also much higher for the lasR rhlR cells in this scenario, and a bit lower for the PA14 cells. The model predicts a coexistence at the point $(10.96 \times 10^7, 10.66 \times 10^7)$. We can see the dynamics of the logistic model for the 10% lasR rhlR case depicted in figure 5.3.(a).

50% lasR rhlR. We get the best parameter vector $P = (\hat{r_1}, \hat{K_1}, \hat{r_2}, \hat{K_2}) = (0.88, 4.00 \times 10^6, 0.35, 13.79 \times 10^7)$. What we can directly see, compared to the 10% case, is the increased growth rate of PA14 cells but a decreased carrying capacity of those cells. The lasR rhlR mutants have a smaller growth rate than in the case with 10% lasR rhlR cells, and a carrying capacity that is very similar to before. The dynamics for this case can be found in figure 5.3.(b).

Figure 5.3.(a)

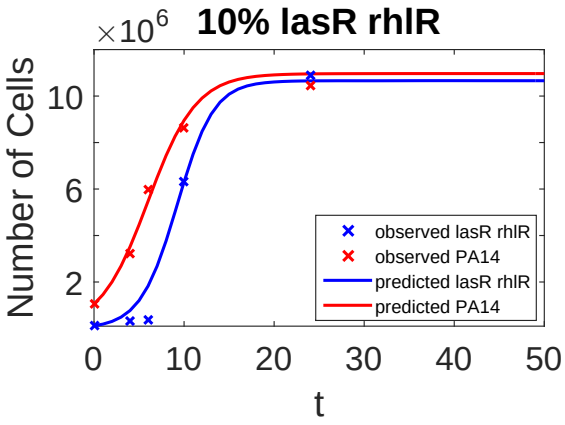

Figure 5.3.(b)

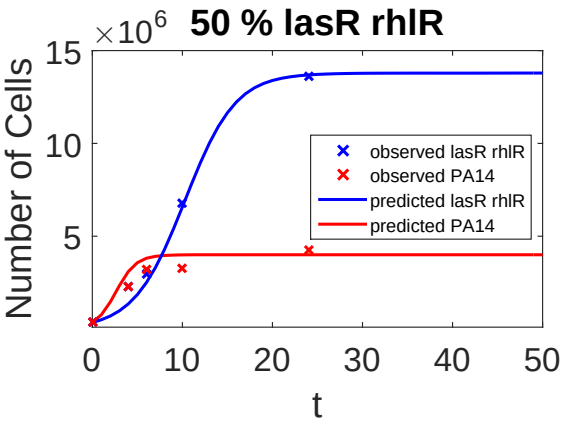

Figure 5.3.(c)

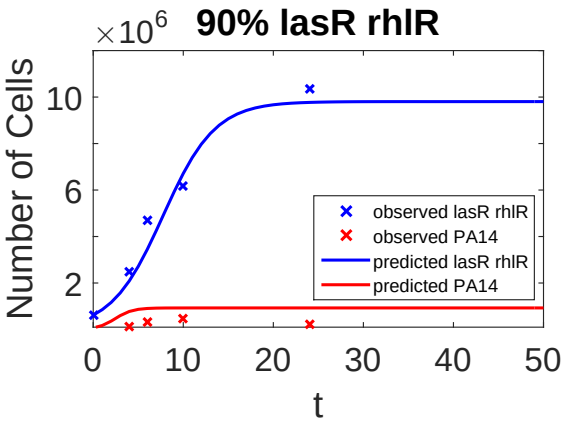

Figure 5.3.: In the three figures we see the dynamics for lasR rhlR mutants and PA14 cells for the best parameter vectors $P = (\hat{r_1}, \hat{K_1}, \hat{r_2}, \hat{K_2}) = (0.37, 10.97 \times 10^7, 0.48, 10.66 \times 10^7)$ for the 10% cheater case, $P = (\hat{r_1}, \hat{K_1}, \hat{r_2}, \hat{K_2}) = (0.88, 4.00 \times 10^6, 0.35, 13.79 \times 10^7)$ for the 50% cheater case and $P = (\hat{r_1}, \hat{K_1}, \hat{r_2}, \hat{K_2}) = (1.04, 9.27 \times 10^5, 0.34, 9.81 \times 10^6)$ for the 90% cheater case of the logistic model (equations 5.18a and 5.18b). Note that the fits look fine, but evaluating with the AIC later shows that this model is not appropriate to explain the dynamics. In figure 5.3.(a), 10% lasR rhlR mutants were growing with 90% PA14 cells at the beginning, in figure 5.3.(b), 50% lasR rhlR mutants were growing with 50% PA14 cells at the beginning, in figure 5.3.(c), 90% lasR rhlR mutants were growing with 10% PA14 cells at the beginning. As explained before, at 5 points of time (after hour $0, 4, 6, 10, 24$) proportions of cells got measured. We converted these proportions to cell numbers, these were average values for several experiments. They are depicted as crosses. The fitting procedure was done with those values and the eleven measurement points (after hour 0,2,3,4,5,6,7,8,9,10,24), which are not depicted, since those values were the sum of lasR rhlR mutants and wildtype cells. The lines show the fits with the optimal parameter vectors found by the optimization with the logistic model.

Figure 5.4.(a)

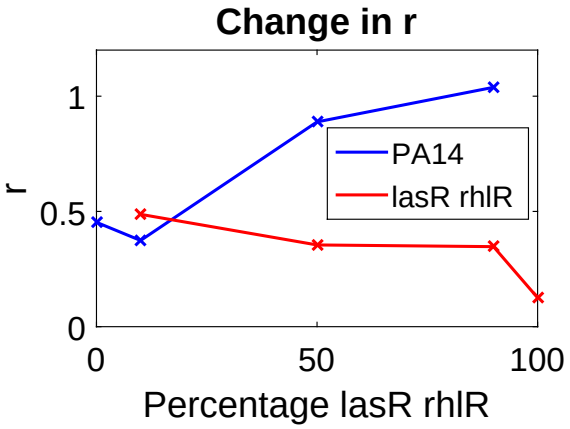

Figure 5.4.(b)

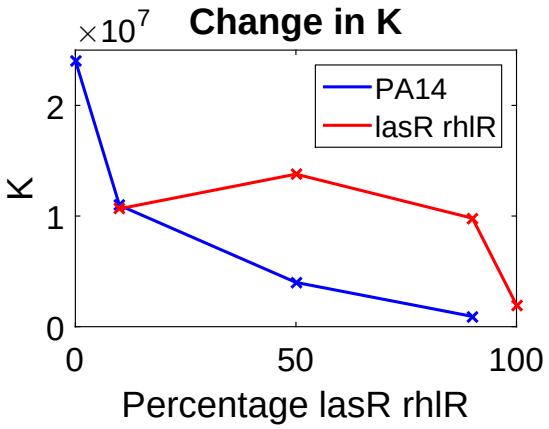

Figure 5.4.: Depicted is the growth rate (figure 5.4.(a)) and change in the carrying capacity (figure 5.4.(b)) depending on the starting conditions for the logistic model (equations 5.18a and 5.18b). We were running five different optimization with the logistic model, where (0%, 10%, 50%, 90% and 100%) lasR rhlR cells were growing at the beginning. The 0% case corresponds to the case where only PA14 was growing, the 100% case corresponds to the case where only lasR rhlR mutants were growing. The crosses are the optimal values found by the optimization and the lines illustrate the trend.

90% lasR rhlR. We get the best parameter vector $P = (\hat{r_1}, \hat{K_1}, \hat{r_2}, \hat{K_2}) = (1.04, 9.27 \times 10^5, 0.34, 9.81 \times 10^6)$. What attracts attention is that the growth rate for the PA14 cells even more increases, where the carrying capacity gets lower. The lasR rhlR mutants have a smaller growth rate and a carrying capacity being more or less the same as in the scenario before. In figure 5.3.(c) we see the associated plot.

Summing up, we see a trend, that the growth rate of PA14 cells is increasing with a higher proportion of lasR rhlR mutants (see figure 5.4.(a)). This could for example be a sign that PA14 cells do not produce many public goods when there is a low proportion of them, and more focus on cell growth. Also it could be a sign that the cell density of PA14 cells is too low such that the expensive gene expression of quorum sensing does not get activated, resulting in a higher growth rate. Moreover we see that the growth rate of lasR rhlR cells decreases in the number of lasR rhlR cells. This effect is not that surprising since this can be well explained by the fact that lasR rhlR cells profit from the PA14 cells, and are very much dependent on the presence of those.

5.2.2. Analysis with Introduced Models

Here, we want to interpret the results from the fitting procedures. We fitted all introduced models to the 10%, 50% and 90% cheater conditions and compared those with the AIC

Percentage of lasR rhlR cells	10%	50%	90%	Parameter
Model 1	481.37	473.50	477.84	4
Model 2	482.78	**468.93**	458.8	6
Model 3	478.67	471.40	463.48	6
Model 4 (i)	**476.40**	475.38	479.84	5
Model 4 (ii)	483.37	469.47	**463.09**	5
Model 5	482.41	472.87	457.48	8
Model 6	484.90	471.06	456.08	8
Model 7	481.83	477.48	460.48	6
Model 8	537.99	473.43	**452.55**	7
Model 9	491.15	490.39	462.45	8
Model 10	540.04	475.43	454.56	8

Table 5.1.: AIC values of the models. The best values for the different scenarios are highlighted in blue color. Note that for the 90% scenario, all models with a value lower than Model 4(ii) where likely to be overfits.

(see table 5.1). In the following the best models for each of the cases (10% lasR rhlR, 50% lasR rhlR and 90% lasR rhlR) are analyzed and interpreted. First the 10% case is analyzed, followed by the 50% case and afterwards the 90% case.

10% lasR rhlR. We see that Model 4(i) has the best AIC value. The model writes

$$\frac{\mathrm{d}x_1}{\mathrm{d}t} = (r_1 + p_1 \frac{x_2}{x_1 + x_2}) x_1 (1 - \frac{x_1}{K_1}) \tag{5.19a}$$

$$\frac{\mathrm{d}x_2}{\mathrm{d}t} = r_2 x_2 (1 - \frac{x_2}{K_2}), \tag{5.19b}$$

and has $(\hat{r_1}, \hat{K_1}, \hat{p_1}, \hat{K_2}, \hat{r_2}) = (0.0003, 1.02 \times 10^7, 2.33, 1.10 \times 10^7, 0.47)$ as the best parameter vector of our fitting procedure.

That this model was chosen by the AIC seems reasonable. As we saw in figure 5.4.(a), the growth rate for PA14 cells looks like an increasing function in the proportions of lasR rhlR cells. When there are 10% lasR rhlR cells and 90% PA14 cells growing at the beginning, there seems to be high exploitation of PA14 cells, and after the proportion of lasR rhlR cells quickly increases, the growth rate of the PA14 cells also increases. An explanation for this could be that with an increasing proportion of cheaters, wildtype cells reduce the production of costly goods, such as autoinducer, and focus on their own growth.
Since the value r_1 is near to zero, it might be sensible to evaluate a model without this

value. We end up with the model

$$\frac{\mathrm{d}x_1}{\mathrm{d}t} = (p_1 \frac{x_2}{x_1 + x_2}) x_1 (1 - \frac{x_1}{K_1}) \tag{5.20a}$$

$$\frac{\mathrm{d}x_2}{\mathrm{d}t} = r_2 x_2 (1 - \frac{x_2}{K_2}). \tag{5.20b}$$

This model is the best model that we evaluated for the 10% lasR rhlR case, and in figure 5.5 we see the associated plots. The best parameter vector is $(\hat{p_1}, \hat{K_1}, \hat{r_2}, \hat{K_2}) = (2.34, 1.02 \times 10^7, 0.47, 1.10 \times 10^7)$.

50% lasR rhlR. The Competitive Lotka Volterra model is the best model for this case. It writes

$$\frac{\mathrm{d}x_1}{\mathrm{d}t} = r_1 x_1 (1 - \frac{x_1 + \alpha_{12} x_2}{K_1}) \tag{5.21a}$$

$$\frac{\mathrm{d}x_2}{\mathrm{d}t} = r_2 x_2 (1 - \frac{x_2 + \alpha_{21} x_1}{K_2}), \tag{5.21b}$$

with the best parameter vector
$(\hat{r_1}, \hat{\alpha_{12}}, \hat{K_1}, \hat{r_2}, \hat{\alpha_{21}}, \hat{K_2}) = (0.72, 0.0003, 3.71 \times 10^6, 0.55, 5.11, 3.34 \times 10^7)$.

When looking at the results, we see that the growth rate for PA14 cells is higher than the growth rate of lasR rhlR cells, and the carrying capacity of lasR rhlR cells is much higher than for the PA14 cells. This time, we have a negative interaction term α_{12} and α_{21}, which describes the negative interaction of lasR rhlR mutants and PA14 cells. We can see, that α_{12} is very near to zero, whereas the value α_{21} is quite high. The value α_{21} could stand for example for the production of toxins as introduced in section 2.3, that PA14 cells produce to eliminate lasR rhlR mutants, leading to a negative interaction term. Since the value α_{12} is very low, we fit this model again, without the parameter value α_{12}, and end up with the model

$$\frac{\mathrm{d}x_1}{\mathrm{d}t} = r_1 x_1 (1 - \frac{x_1}{K_1}) \tag{5.22a}$$

$$\frac{\mathrm{d}x_2}{\mathrm{d}t} = r_2 x_2 (1 - \frac{x_2 + \alpha_{21} x_1}{K_2}). \tag{5.22b}$$

The best parameter vector reads
$(\hat{r_1}, \hat{K_1}, \hat{r_2}, \hat{\alpha_{21}}, \hat{K_2}) = (0.71, 3.66 \times 10^6, 0.56, 5.97, 3.65 \times 10^7)$. This model has the best AIC value for the 50% lasR rhlR case. In figure 5.6, the results are depicted.

Figure 5.5.(a)

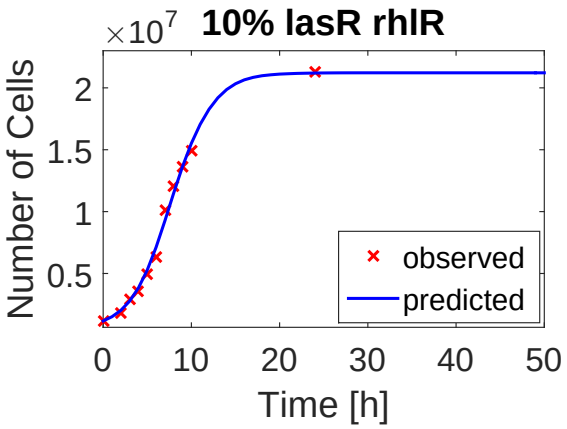

Figure 5.5.(b)

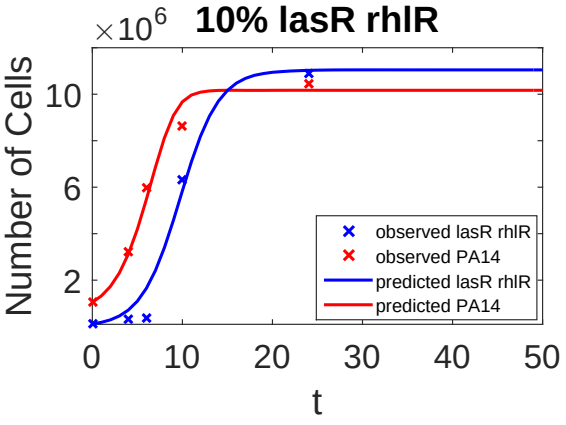

Figure 5.5.(c)

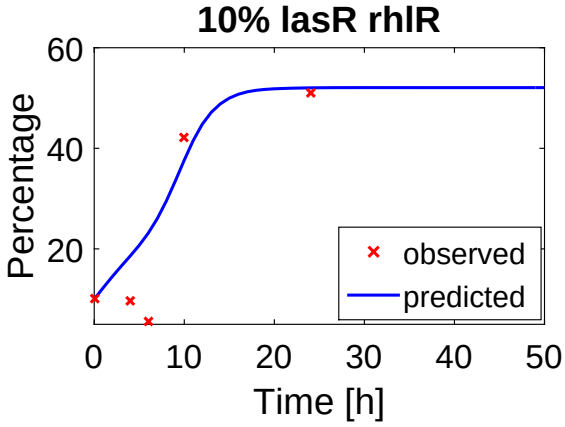

Figure 5.5.: In figure 5.5.(a), we see the fit of the sum of cells of lasR rhlR mutants and wildtype cells for the best model in the 10% lasR rhlR case (equations 5.20a and 5.20b), with the best parameter vector $(\hat{p_1}, \hat{K_1}, \hat{r_2}, \hat{K_2}) = (2.34, 1.02 \times 10^7, 0.47, 1.10 \times 10^7)$. The red crosses are the eleven measurement points where the sum of cheater and wildtype cells was measured (after hour 0,2,3,4,5,6,7,8,9,10,24).
In figure 5.5.(b), we see the associated dynamics of lasR rhlR mutants and PA14 cells. The red and blue crosses are the observed proportions which were converted to cell numbers (after hour $0, 4, 6, 10, 24$).
In figure 5.5.(c), we see the development of the lasR rhlR percentage over time. The red crosses are the observed proportions (after hour $0, 4, 6, 10, 24$).

Figure 5.6.(a)

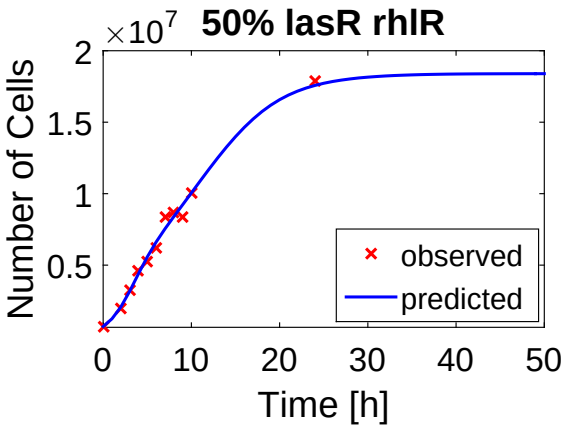

Figure 5.6.(b)

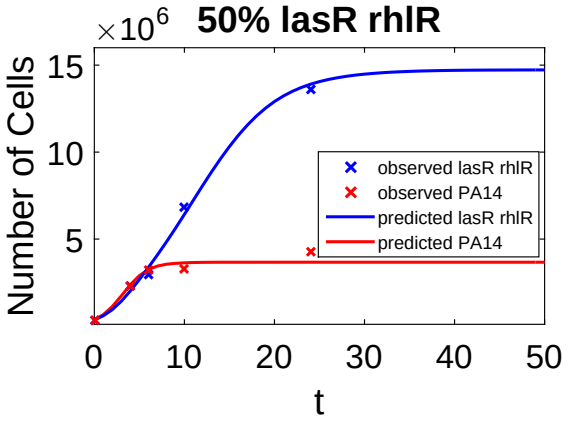

Figure 5.6.(c)

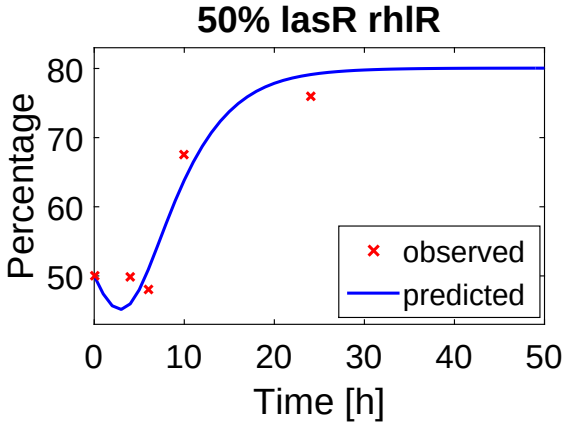

Figure 5.6.: In figure 5.6.(a), we see the fit of the sum of cells of lasR rhlR mutants and wildtype cells for the best model in the 50% lasR rhlR case (equations 5.22a and 5.22b), with the best parameter vector $(\hat{r_1}, \hat{K_1}, \hat{r_2}, \hat{\alpha_{21}}, \hat{K_2}) = (0.71, 3.66 \times 10^6, 0.56, 5.97, 3.65 \times 10^7)$. The red crosses are the eleven measurement points where the sum of cheater and wildtype cells was measured (after hour 0,2,3,4,5,6,7,8,9,10,24).
In figure 5.6.(b), we see the associated dynamics of lasR rhlR mutants and PA14 cells. The red and blue crosses are the observed proportions which were converted to cell numbers (after hour $0, 4, 6, 10, 24$).
In figure 5.6.(c), we see the development of the lasR rhlR percentage over time. The red crosses are the observed proportions (after hour $0, 4, 6, 10, 24$).

90% lasR rhlR. We get the following model as the best one:

$$\frac{\mathrm{d}x_1}{\mathrm{d}t} = r_1 x_1 (1 - \frac{x_1 + \alpha_{12} x_2}{K_1}) \tag{5.23a}$$

$$\frac{\mathrm{d}x_2}{\mathrm{d}t} = (r_2 + p\frac{x_1}{x_1 + x_2}) x_2 (1 - \frac{x_2 - \alpha_{21} x_1}{K_2}). \tag{5.23b}$$

This model seems to be the best according to the model evaluation. We performed the fitting procedure for thousands of iterations and got several very similar points, which indicated identifiablity. But when we look at figure 5.7, we see that this fit is likely to be an overfit.
Let us look at the models that are fit appropriately, and that have the best model evaluation. As best model of the appropriate fitted models we get the same one as in the 10% lasR rhlR case, just the reversed model

$$\frac{\mathrm{d}x_1}{\mathrm{d}t} = r_1 x_1 (1 - \frac{x_1}{K_1}) \tag{5.24a}$$

$$\frac{\mathrm{d}x_2}{\mathrm{d}t} = (p_2\frac{x_1}{x_1 + x_2}) x_2 (1 - \frac{x_2}{K_2}), \tag{5.24b}$$

with the best parameter vector $(\hat{r_1}, \hat{K_1}, \hat{p_2}, K_2) = (2.94, 4.34 \times 10^5, 1.00, 1.12 \times 10^7)$. Since the other models were much better according to the AIC but were likely to be overfitted, we do not interpret this case, but we show the fits of this model in figure 5.8 and show the profiles in the next section. Note that the percentage was also not fitted properly for this case.

5.3. Uncertainty Analysis using the Profile Likelihood

In this section, we want to look at the profiles of our best models. To analyze if our parameters are identifiable, we calculate the confidence intervals for the parameters. We look at the best models of the different cases, and start again with the 10% lasR rhlR case, then the 50% case and afterwards the 90% case. If the confidence intervals are finite, the parameters are identifiable [1].
10% lasR rhlR. We got the best parameter vector as $(\hat{p_1}, \hat{K_1}, \hat{r_2}, \hat{K_2}) = (2.34, 1.02 \times 10^7, 0.47, 1.10 \times 10^7)$. After calculating the 95% confidence intervals, we get $\hat{p_1} \in [1.81, 2.93]$, $\hat{K_1} \in [9.06 \times 10^6, 1.14 \times 10^7]$, $\hat{r_2} \in [0.44, 0.50]$, $\hat{K_2} \in [1.01 \times 10^7, 1.20 \times 10^7]$, and we see the associated plots in figure 5.9.
50% lasR rhlR. We got the best parameter vector as $(\hat{r_1}, \hat{K_1}, \hat{r_2}, \hat{\alpha_{21}}, \hat{K_2}) = (0.71, 3.66 \times 10^6, 0.56, 5.97, 3.65 \times 10^7)$. After calculating the 95% confidence intervals, we get $\hat{r_1} \in [0.57, 0.92]$, $\hat{K_1} \in [3.13 \times 10^6, 4.33 \times 10^6]$, $\hat{r_2} \in [0.44, 0.65]$, $\hat{\alpha_{21}} \in [1.64, 15.47]$, $\hat{K_2} \in$

Figure 5.7.(a)

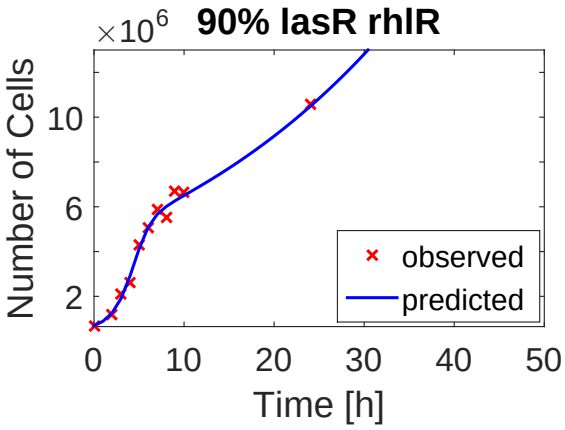

Figure 5.7.(b)

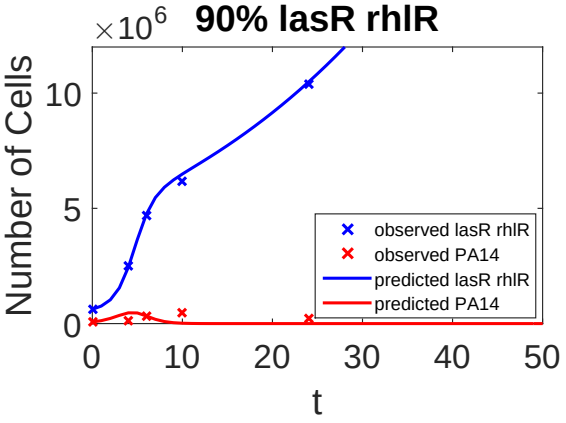

Figure 5.7.(c)

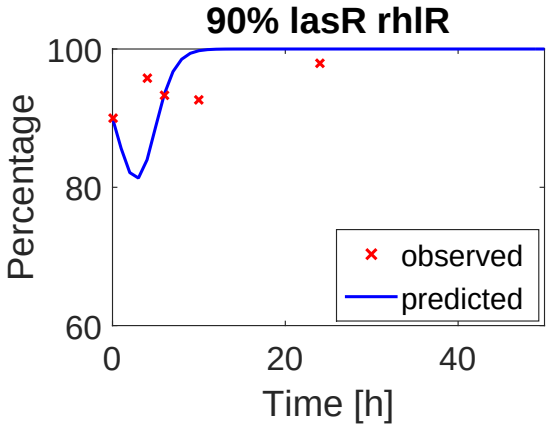

Figure 5.7.: In figure 5.7.(a), we see the fit of the sum of cells of lasR rhlR mutants and wildtype cells for the best model in the 90% lasR rhlR case (equations 5.23a and 5.23b). The red crosses are the eleven measurement points where the sum of cheater and wildtype cells was measured (after hour 0,2,3,4,5,6,7,8,9,10,24). In figure 5.7.(b), we see the associated dynamics of lasR rhlR mutants and PA14 cells. The red and blue crosses are the observed proportions which were converted to cell numbers (after hour $0, 4, 6, 10, 24$).
In figure 5.7.(c), we see the development of the lasR rhlR percentage over time. The red crosses are the observed proportions (after hour $0, 4, 6, 10, 24$). The dynamics that this model predicts are likely to be overfits.

Figure 5.8.(a)

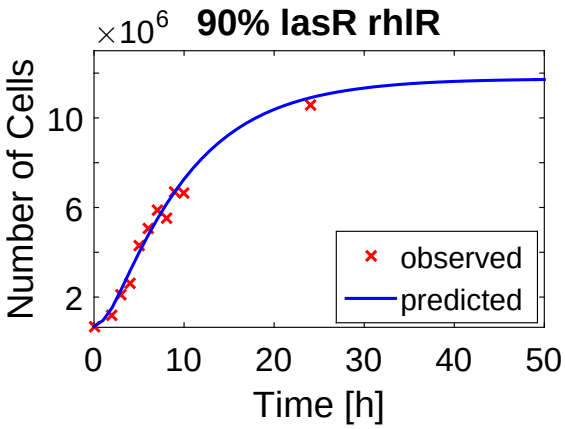

Figure 5.8.(b)

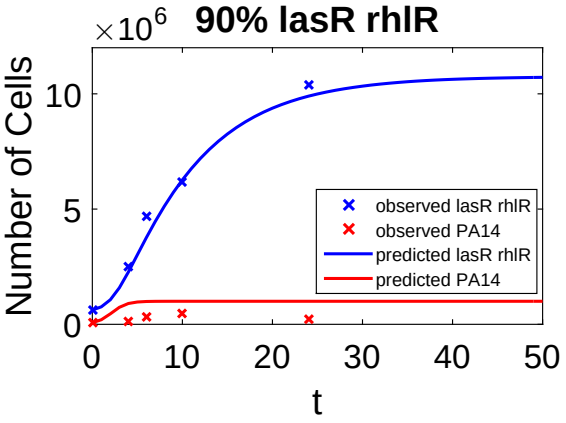

Figure 5.8.(c)

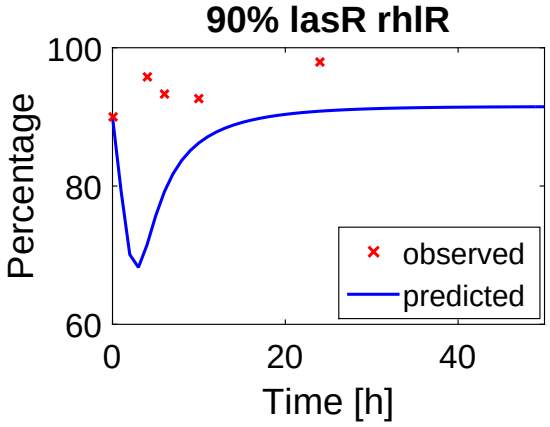

Figure 5.8.: In figure 5.8.(a), we see the fit of the sum of cells of lasR rhlR mutants and wildtype cells for the best model in the 90% lasR rhlR case (equations 5.24a and 5.24b), with the best parameter vector $(\hat{r_1}, \hat{K_1}, \hat{p_2}, K_2) = (2.94, 4.34 \times 10^5, 1.00, 1.12 \times 10^7)$. The red crosses are the eleven measurement points where the sum of cheater and wildtype cells was measured (after hour 0,2,3,4,5,6,7,8,9,10,24).
In figure 5.8.(b), we see the associated dynamics of lasR rhlR mutants and PA14 cells. The red and blue crosses are the observed proportions which were converted to cell numbers (after hour $0, 4, 6, 10, 24$).
In figure 5.8.(c), we see the development of the lasR rhlR percentage over time. The red crosses are the observed proportions (after hour $0, 4, 6, 10, 24$).

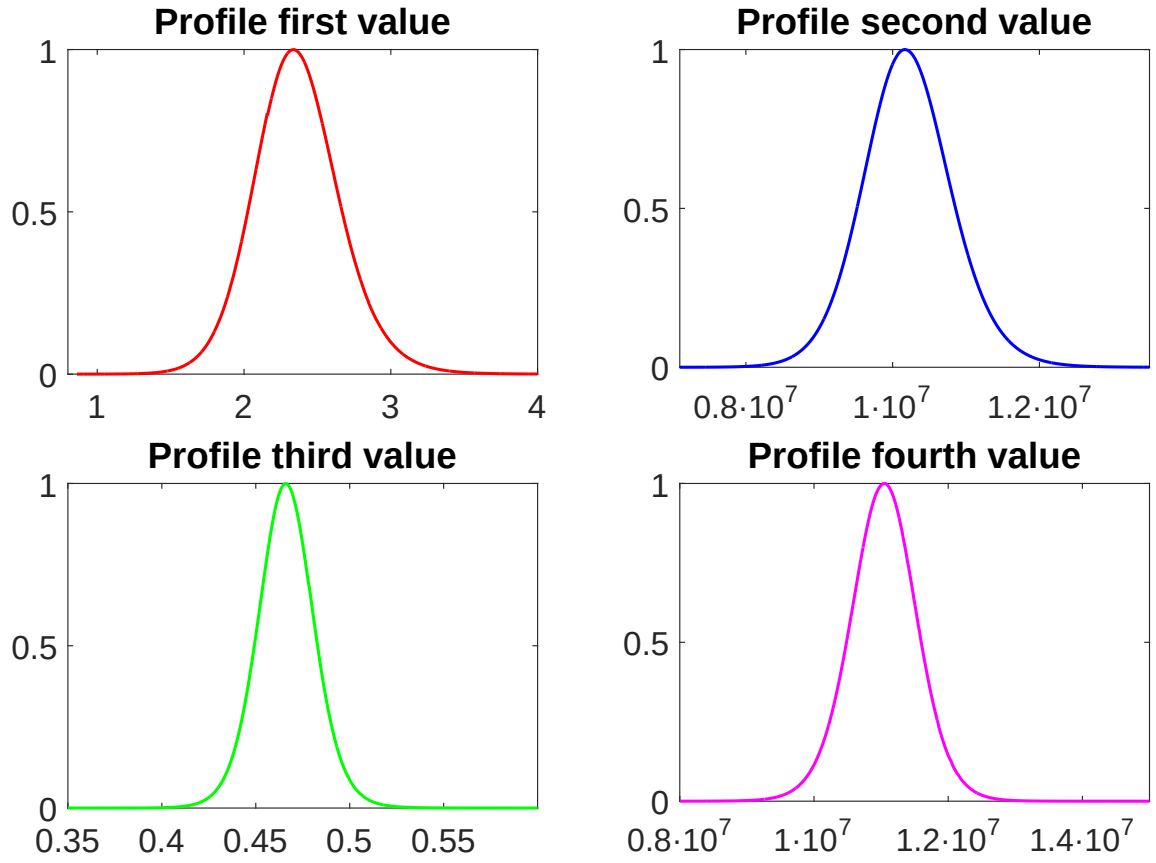

Figure 5.9.: We see the profiles for the 10% lasR rhlR scenario. The best parameter vector was $(\hat{p_1}, \hat{K_1}, \hat{r_2}, \hat{K_2}) = (2.34, 1.02 \times 10^7, 0.47, 1.10 \times 10^7)$ with 95% confidence intervals as $\hat{p_1} \in [1.81, 2.93]$, $\hat{K_1} \in [9.06 \times 10^6, 1.14 \times 10^7]$, $\hat{r_2} \in [0.44, 0.50]$, $\hat{K_2} \in [1.01 \times 10^7, 1.20 \times 10^7]$.

$[2.01 \times 10^7, 5.93 \times 10^7]$. We can see the associated plots in figure 5.10.

90% lasR rhlR. We got the best parameter vector as $(\hat{r_1}, \hat{K_1}, \hat{p_2}, K_2) = (2.94, 4.34 \times 10^5, 1.00, 1.12 \times 10^7)$. Calculating the confidence intervals, the results are $\hat{r_1} \in [1.60, 6.63]$, $\hat{K_1} \in [1.78 \times 10^5, 8.47 \times 10^5]$, $\hat{p_2} \in [0.45, 1.82]$, $\hat{K_2} \in [1.03 \times 10^7, 1.25 \times 10^7]$. The associated plots can be seen in figure 5.11.

Since all of the confidence intervals are finite, all of the parameters are identifiable.

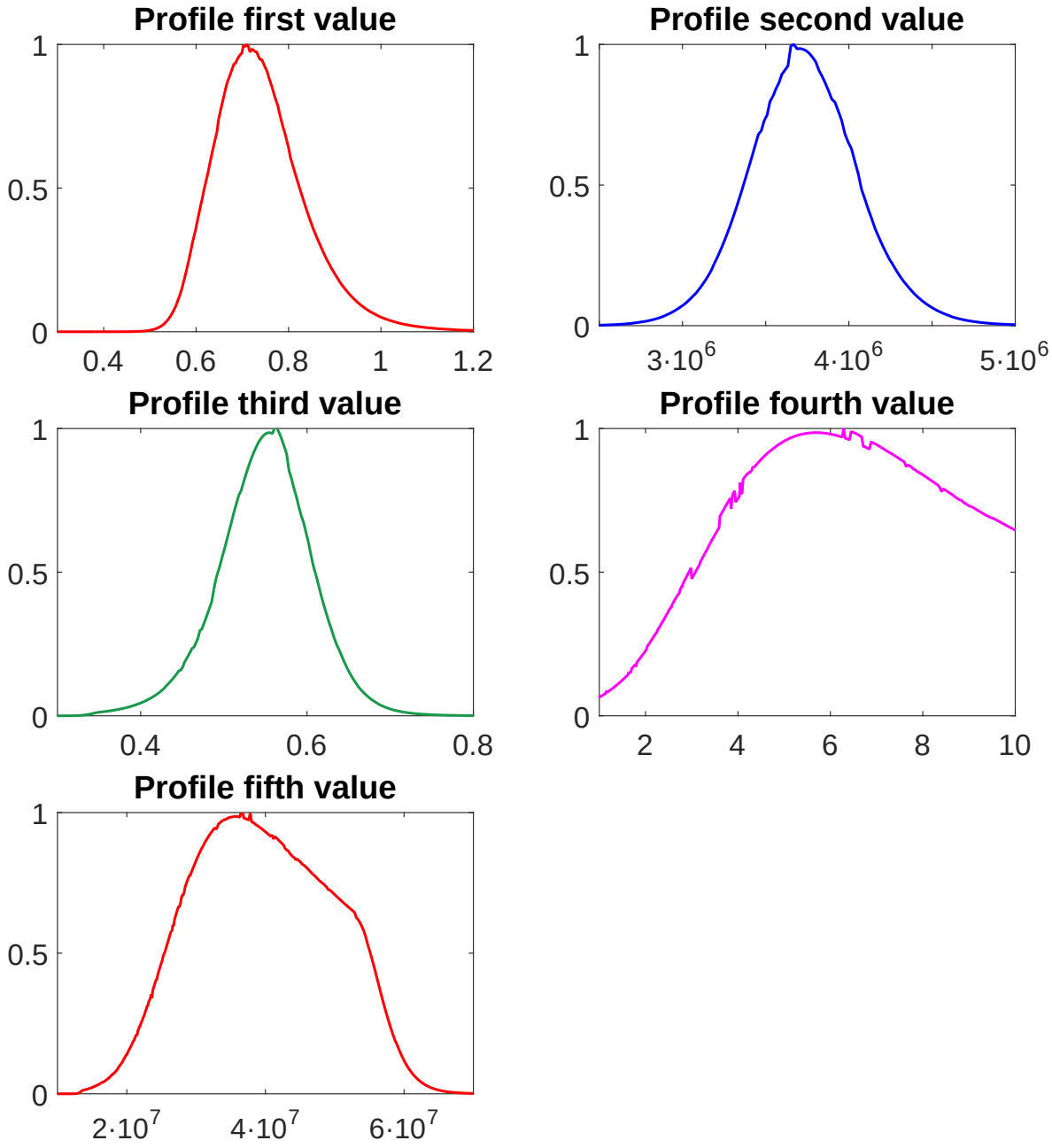

Figure 5.10.: We see the profiles for the 50% lasR rhlR scenario. The best parameter vector was $(\hat{r_1}, \hat{K_1}, \hat{r_2}, \hat{\alpha_{21}}, \hat{K_2}) = (0.71, 3.66 \times 10^6, 0.56, 5.97, 3.65 \times 10^7)$ with 95% confidence intervals as $\hat{r_1} \in [0.57, 0.92]$, $\hat{K_1} \in [3.13 \times 10^6, 4.33 \times 10^6]$, $\hat{r_2} \in [0.44, 0.65]$, $\hat{\alpha_{21}} \in [1.64, 15.47]$, $\hat{K_2} \in [2.01 \times 10^7, 5.93 \times 10^7]$.

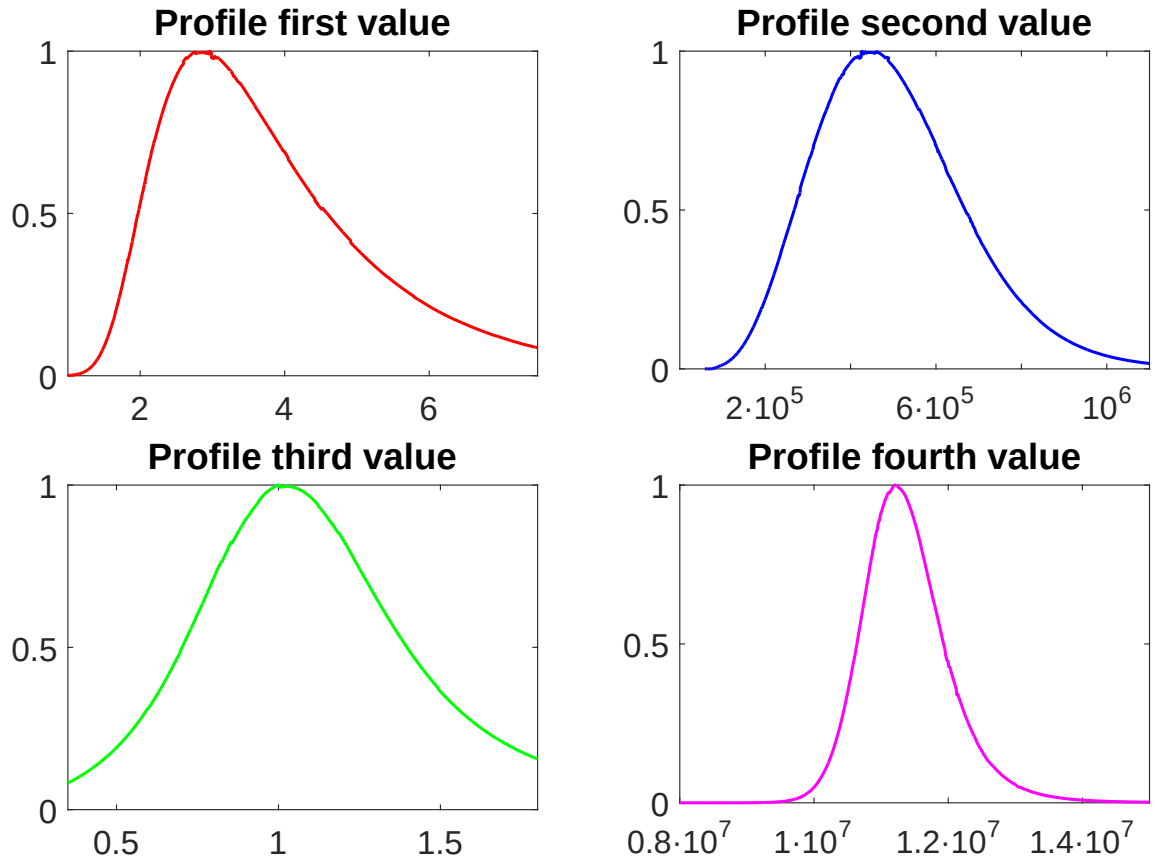

Figure 5.11.: We see the profiles for the 90% lasR rhlR scenario. The best parameter vector was $(\hat{r_1}, \hat{K_1}, \hat{p_2}, K_2) = (2.94, 4.34 \times 10^5, 1.00, 1.12 \times 10^7)$ with 95% confidence intervals as $\hat{r_1} \in [1.60, 6.63]$, $\hat{K_1} \in [1.78 \times 10^5, 8.47 \times 10^5]$, $\hat{p_2} \in [0.45, 1.82]$, $\hat{K_2} \in [1.03 \times 10^7, 1.25 \times 10^7]$.

6. Future Work and Discussion

Here we want to discuss our findings and outline further work that can be done on this topic. In this work we used mathematical modeling to analyze the interaction between *Pseudomonas aeruginosa* wildtype cells and quorum sensing cheaters. For the case where only cheaters and wildtype cells were growing alone, we took the logistic model to explain the dynamics. Moreover we analyzed cases where cheater cells and wildtype cells were growing together for different starting conditions. For the 10% cheater case, we saw that the cheater had a high growth rate, which can be explained by their exploitative behavior. With an increasing proportion of cheater cells, we found that the growth rate of PA14 cells increases. This could be explained by the fact that wildtype cells prevent this exploitative behavior when the amount of cheater increases, for example due to reducing the production of autoinducers and using more energy for their own growth. For the 50% cheater case, we saw that a model similar to the Competitive Lotka Volterra equations fitted the observed data best. We estimated a parameter value α_{12} for the cheater cells, which accounts for the interaction with the wildtype cells. This could be due to the production of toxins by wildtype cells that penalizes the cheater cells. When we analyzed the 90% lasR rhlR case, we saw that the model with the best AIC evaluation was likely to be an overfit. It is possible that we picked a model with too many degrees of freedom in this case.

In our studies, we focused on the case where no stress was added. In this case, under normal control conditions, the outcome was a coexistence of wildtype and cheater cells, where the proportion of cheater cells was increasing in time, until the system settled at a stable point. In reality, however, cells could be exposed to stress from the environment, such as oxidative stress (e.g. H_2O_2). As we mentioned before, a stressor selects for cells with an active quorum sensing system, and cheater cells like lasR rhlR do not have a proper functioning quorum sensing system. Thus, cheaters are likely to be more vulnerable under stress. In future, it may be interesting to find mathematical models that can explain the dynamics of cheater and wildtype cells exposed to stressors, to also incorporate these additional factors.

A. Appendix

A.1. Stationary Points

Model 3
$P_1 = (0,0),\ P_2 = (\frac{-(K_2 p_1 + K_2 r_1)}{r_1}, K_2),\ P_3 = (K_1, \frac{-(K_1 p_2 + K_1 r_2)}{r_2}),$
$P_4 = (K_1, 0),\ P_5 = (0, K_2),\ P_6 = (K_1, K_2)$

Model 4 (i)
$P_1 = (0,0),\ P_2 = (\frac{-(K_2 p_1 + K_2 r_1)}{r_1}, K_2),\ P_3 = (K_1, 0),\ P_4 = (0, K_2),\ P_5 = (K_1, K_2)$

Model 4 (ii)
$P_1 = (0,0),\ P_2 = (K_1, \frac{-(K_1 p_2 + K_1 r_2)}{r_2}),\ P_3 = (K_1, 0),\ P_4 = (0, K_2),\ P_5 = (K_1, K_2)$

Model 5
$P_1 = (\frac{-(K_1 - K_2\alpha_{12})}{\alpha_{12}\alpha_{21} - 1}, \frac{-(K_2 - K_1\alpha_{21})}{\alpha_{12}\alpha_{21} - 1}),\ P_2 = (\frac{K_2(p_1 + r_1)}{\alpha_{21}p_1 - r_1 + \alpha_{21}r_1}, \frac{-K_2 r_1}{\alpha_{21}p_1 - r_1 + \alpha_{21}r_1}),$
$P_3 = (\frac{-K_1 r_2}{\alpha_{12}p_2 - r_2 + \alpha_1 r_2}, \frac{K_1 p_2 + K_1 r_2}{\alpha_{12}p_2 - r_2 + \alpha_{12}r_2}),$
$P_4 = (0,0),\ P_5 = (K_1, 0),\ P_6 = (0, K_2)$

Model 6
$P_1 = (\frac{-(K_1 - K_2\alpha_{12})}{\alpha_{12}\alpha_{21} - 1}, \frac{-(K_2 - K_1\alpha_{21})}{\alpha_{12}\alpha_{21} - 1}),\ P_2 = (\frac{-K_1 r_2}{\alpha_{12}p_2 - r_2 + \alpha_{12}r_2}, \frac{(K_1 p_2 + K_1 r_2)}{\alpha_{12}p_2 - r_2 + \alpha_{12}r_2}),\ P_3 = (0,0),\ P_4 = (K_1, 0),\ P_5 = (0, K_2)$

Model 7
$P_1 = (\frac{K_1 - K_2\alpha_{12}}{\alpha_{12}\alpha_{21} + 1}, \frac{K_2 + K_1\alpha_{21}}{\alpha_{12}\alpha_{21} + 1}),\ P_2 = (0,0), P_3 = (K_1, 0),\ P_4 = (0, K_2)$

Model 8
$P_1 = (\frac{K_1 - K_2\alpha_{12}}{\alpha_{12}\alpha_{21} + 1}, \frac{K_2 + K_1\alpha_{21}}{\alpha_{12}\alpha_{21} + 1}),\ P_2 = (\frac{-K_1 r_2}{\alpha_{12}p_2 - r_2 + \alpha_{12}r_2}, \frac{K_1 p_2 + K_1 r_2}{\alpha_{12}p_2 - r_2 + \alpha_{12}r_2}),$
$P_3 = (0,0),\ P_4 = (K_1, 0),\ P_5 = (0, K_2)$

Model 9
$P_1 = (\frac{-K_2 r_1}{p_1+r_1-\alpha_{21} r_1}, \frac{K_2 p_1+K_2 r_1}{p_1+r_1-\alpha_{21} r_1}),\ P_2 = (\frac{-(K_1-K_2\alpha_{12})}{\alpha_{12}\alpha_{21}-1},\ \frac{-(K_2-K_1\alpha_{21})}{\alpha_{12}\alpha_{21}-1}),$
$P_3 = (\frac{-K_1 r_2}{\alpha_{12} p_2-r_2+\alpha_{12} r_2}, \frac{K_1 p_2+K_1 r_2}{\alpha_{12} p_2-r_2+\alpha_{12} r_2}),\ P_4 = (0,0),\ P_5 = (K_1,0),\ P_6 = (0,K_2)$

Model 10
$P_1 = (\frac{-K_2 r_1}{p_1+r_1+\alpha_{21} r_1}, \frac{K_2 p_1+K_2 r_1}{p_1+r_1+\alpha_{21} r_1}),\ P_2 = (\frac{K_1-K_2\alpha_{12}}{\alpha_{12}\alpha_{21}+1}, \frac{K_2+K_1\alpha_{21}}{\alpha_{12}\alpha_{21}+1}),$
$P_3 = (\frac{-K_1 r_2}{(\alpha_{12} p_2-r_2+\alpha_{12} r_2)}, \frac{K_1 p_2+K_1 r_2}{\alpha_{12} p_2-r_2+\alpha_{12} r_2}),\ P_4 = (0,0),\ P_5 = (K_1,0),\ P_6 = (0,K_2)$

A.2. List of Figures

Bibliography

[1] Raue A, Becker V, Klingmüller U, and Timmer J. Identifiability and observability analysis for experimental design in nonlinear dynamical models. *Chaos: An Interdisciplinary Journal of Nonlinear Science*, 20(4):045105, 2010.

[2] Fuqua C, Winans SC, and Greenberg EP. Census and consensus in bacterial ecosystems: the LuxR-LuxI family of quorum-sensing transcriptional regulators. *Annual Reviews in Microbiology*, 50(1):727–751, 1996.

[3] Kuttler C. Mathematical ecology - lecture notes. *TU München*, 2014.

[4] Reimmann C, Beyeler M, Latifi A, Winteler H, Foglino M, Lazdunski A, and Haas D. The global activator GacA of pseudomonas aeruginosa PAO positively controls the production of the autoinducer N-butyryl-homoserine lactone and the formation of the virulence factors pyocyanin, cyanide, and lipase. *Molecular microbiology*, 24(2):309–319, 1997.

[5] Stover CK, Pham XQ, Erwin AL, Mizoguchi SD, Warrener P, Hickey MJ, Brinkman FSL, Hufnagle WO, Kowalik DJ, and Lagrou M. Complete genome sequence of pseudomonas aeruginosa PAO1, an opportunistic pathogen. *Nature*, 406(6799):959–964, 2000.

[6] Waters CM and Bassler BL. Quorum sensing: cell-to-cell communication in bacteria. *Annu. Rev. Cell Dev. Biol.*, 21:319–346, 2005.

[7] Arrowsmith D and Place CM. *Dynamical systems: differential equations, maps, and chaotic behaviour*, volume 5. CRC Press, 1992.

[8] Box GEP, Jenkins GW, and Reinsel GC. *Time series analysis: forecasting and control*, volume 734. John Wiley & Sons, 2011.

[9] Müller J. Mathematical models in biology. *TU München*, SS 2014.

[10] Dockery JD and Keener JP. A mathematical model for quorum sensing in pseudomonas aeruginosa. *Bulletin of mathematical biology*, 63(1):95–116, 2001.

[11] Anguige K, King JR, and Ward JP. A multi-phase mathematical model of quorum sensing in a maturing pseudomonas aeruginosa biofilm. *Mathematical biosciences*, 203(2):240–276, 2006.

[12] Rumbaugh KP, Trivedi U, Watters C, Burton-Chellew MN, Diggle SP, and West SA. Kin selection, quorum sensing and virulence in pathogenic bacteria. *Proceedings of the Royal Society B: Biological Sciences*, 2012.

[13] Chan M. Antimicrobial resistance in the european union and the world. *World Health Organization*, 2012.

[14] Schuster M, Sexton DJ, Diggle SP, and Greenberg EP. Acyl-homoserine lactone quorum sensing: from evolution to application. *Annual review of microbiology*, 67:43–63, 2013.

[15] Wang M, Schaefer AL, Dandekar AA, and Greenberg EP. Quorum sensing and policing of pseudomonas aeruginosa social cheaters. *Proceedings of the National Academy of Sciences*, 112(7):2187–2191, 2015.

[16] Maciá MD, Blanquer D, Togores B, Sauleda J, Pérez JL, and Oliver A. Hypermutation is a key factor in development of multiple-antimicrobial resistance in pseudomonas aeruginosa strains causing chronic lung infections. *Antimicrobial agents and chemotherapy*, 49(8):3382–3386, 2005.

[17] Willcox MDP, Zhu H, Conibear TCR, Hume EBH, Givskov M, Kjelleberg S, and Rice SA. Role of quorum sensing by pseudomonas aeruginosa in microbial keratitis and cystic fibrosis. *Microbiology*, 154(8):2184–2194, 2008.

[18] Taga ME and Bassler BL. Chemical communication among bacteria. *Proceedings of the National Academy of Sciences*, 100(suppl 2):14549–14554, 2003.

[19] Williams P. Quorum sensing, communication and cross-kingdom signalling in the bacterial world. *Microbiology*, 153(12):3923–3938, 2007.

[20] Seed PC, Passador L, and Iglewski BH. Activation of the pseudomonas aeruginosa lasi gene by LasR and the pseudomonas autoinducer PAI: an autoinduction regulatory hierarchy. *Journal of bacteriology*, 177(3):654–659, 1995.

[21] García-Contreras R, Nuñez-López L, Jasso-Chávez R, Kwan BW, Belmont JA, Rangel-Vega A, Maeda T, and Wood TK. Quorum sensing enhancement of the stress response promotes resistance to quorum quenching and prevents social cheating. *The ISME journal*, 2014.

[22] Finch RG, Pritchard DI, Bychroft BW, Williams P, and Stewart GSAB. Leading articles-quorum sensing: A novel target for anti-infective therapy. *Journal of Antimicrobial Chemotherapy*, 42(5):569–571, 1998.

[23] Rulands S, Reichenbach T, and Frey E. Threefold way to extinction in populations of cyclically competing species. *Journal of Statistical Mechanics: Theory and Experiment*, 2011(01):L01003, 2011.

[24] Schauder S and Bassler BL. The languages of bacteria. *Genes & Development*, 15(12):1468–1480, 2001.

[25] Davies SC and Gibbens N. Uk five year antimicrobial resistance strategy 2013 to 2018. *Department of Health, London*, 2013.

[26] Brown SP, West SA, Diggle SP, and Griffin AS. Social evolution in micro-organisms and a trojan horse approach to medical intervention strategies. *Philosophical Transactions of the Royal Society B: Biological Sciences*, 364(1533):3157–3168, 2009.

[27] Diggle SP, Griffin AS, Campbell GS, and West SA. Cooperation and conflict in quorum-sensing bacterial populations. *Nature*, 450(7168):411–414, 2007.

[28] Twining SS, Kirschner SE, Mahnke LA, and Frank DW. Effect of pseudomonas aeruginosa elastase, alkaline protease, and exotoxin A on corneal proteinases and proteins. *Investigative ophthalmology & visual science*, 34(9):2699–2712, 1993.

[29] Rutherford ST and Bassler BL. Bacterial quorum sensing: its role in virulence and possibilities for its control. *Cold Spring Harbor Perspectives in Medicine*, 2(11), 2012.

[30] Czárán T and Hoekstra RF. Microbial communication, cooperation and cheating: quorum sensing drives the evolution of cooperation in bacteria. *PloS one*, 4(8), 2009.

[31] Köhler T, van Delden C, Curty LK, Hamzehpour MM, and Pechere JC. Overexpression of the MexEF-OprN multidrug efflux system affects cell-to-cell signaling in pseudomonas aeruginosa. *Journal of Bacteriology*, 183(18):5213–5222, 2001.

[32] Coleman TF and Li Y. An interior trust region approach for nonlinear minimization subject to bounds. *SIAM Journal on optimization*, 6(2):418–445, 1996.

[33] Friman VP, Diggle SP, and Buckling A. Protist predation can favour cooperation within bacterial species. *Biology letters*, 9(5), 2013.